# Selective dehydration of glycerol on copper based catalysts

Chimentão, R. J.; Hirunsit, P.; Torres, C. S.; Ordoño, M. Borges; Urakawa, A.; Fierro, J. L.G.; Ruiz, D.

**DOI**
10.1016/j.cattod.2020.09.031

**Publication date**
2020

**Document Version**
Accepted author manuscript

**Published in**
Catalysis Today

**Citation (APA)**
Chimentão, R. J., Hirunsit, P., Torres, C. S., Ordoño, M. B., Urakawa, A., Fierro, J. L. G., & Ruiz, D. (2020). Selective dehydration of glycerol on copper based catalysts. *Catalysis Today*, *367*, 58-70. https://doi.org/10.1016/j.cattod.2020.09.031

# Selective dehydration of glycerol on copper based catalysts

R. J. Chimentão[1,§,*], P. Hirunsit[2,§], C. S. Torres[1], M. Borges Ordoño[3], A. Urakawa[3,4], J.L.G. Fierro[5], D. Ruiz[1]

[1] *Universidad de Concepción, Facultad de Ciencias Químicas, Edmundo Larenas 129, Casilla 160C, Chile*

[2] *National Nanotechnology Center (NANOTEC), National Science and Technology Development Agency (NSTDA), Pathum Thani, 12120 Thailand*

[3] *Institute of Chemical Research of Catalonia (ICIQ), The Barcelona Institute of Science and Technology, Av. Països Catalans 16, 43007 Tarragona, Spain*

[4] *Catalysis Engineering, Department of Chemical Engineering, Delft University of Technology, Van der Maasweg 9, 2629 HZ Delft, The Netherlands*

[5] *Institute of Catalysis and Petrochemistry (CSIC), Cantoblanco, 28049, Madrid, Spain*

§ These authors contributed equally

* Corresponding author: *rchimenton@udec.cl*

Phone number: +56 (041) 220-3354

**Abstract**

Glycerol is produced in large quantities as a byproduct of biodiesel, and among others hydroxyacetone (acetol) is an important commodity obtained from glycerol. Metallic Cu has been identified as active site for the dehydration of glycerol to hydroxyacetone and acid and metal sites are known to influence the catalytic performance.

In this study, dehydration of glycerol over 5 wt.% copper supported on $\gamma$-$Al_2O_3$, $ZrO_2$ and $SiO_2$ was investigated. Catalysts were characterized by $N_2$ physisorption, $H_2$-TPR, $NH_3$-TPD, $N_2O$ chemisorption, XPS, XRD, FTIR of pyridine adsorption. Cu/$ZrO_2$ exhibited the highest hydroxyacetone yield at 20% of glycerol conversion and the highest apparent reaction rate. The superior activity of Cu/$ZrO_2$ was attributed to the highly acidic, both Lewis and Brönsted acidic, nature of the support and positive roles of the interfacial sites. The Weisz-Prater (WP) criterion was applied to confirm the absence of intraparticle diffusion limitations. It was assumed spherical particles and first order reaction. The WP value obtained in the worst scenario was less than 0.3 ensuring no diffusion limitation.

Complementary DFT study indicates that both glycerol and hydroxyacetone interact significantly stronger on Cu/$\gamma$-$Al_2O_3$ and Cu/$ZrO_2$ compared to metallic Cu, suggesting that the active sites are at the interface of Cu particles and the acidic support.

*Key-words: Glycerol, Dehydration, Hydroxyacetone, Copper, Catalyst*

## 1. Introduction

Glycerol is a relevant bio-renewable compound for its increasing availability, since it is produced in large quantities as a by-product during the transesterification of ester to obtain biodiesel. The glycerol produced represents 10% of the total mass of the biodiesel production. Glycerol is a compound of great importance already in our daily lives, e.g. in food industry, due to its non-toxic nature [2], and it could become one of the most important building blocks for chemical production in the biorefinery [1]. Related to the latter, a variety of catalytic conversion routes to valorise the molecule, such as hydrogenolysis to propylene glycol [3], catalytic reforming [4], cracking for the production of olefins and light parafins [5], oxidation towards acids (dihydroxyacetone, tartronic acid, glyceric acid) [6], oligomerization, polymerization towards glycerol monoesters [7], transesterification to monoglycerides [8], dehydration to acrolein or hydroxyacetone [9], carboxylation to glycerol carbonate [10], have been reported to date.

This work focuses on the selective dehydration of glycerol to hydroxyacetone. Hydroxyacetone is an interesting building block due to its extremely reactive multifunctional structure which contains hydroxyl and carbonyl functional groups. Particularly, it is an attractive intermediate of 1,2-propanediol (1,2-PDO) which is used for the synthesis of resins, liquid detergents, cosmetics, and pharmaceuticals and can be produced by hydrogenation of hydroxyacetone. 1,2-PDO is currently produced from fossil fuel derived propylene oxide. The catalytic process for the conversion of glycerol to 1,2-PDO requires external hydrogen supply. The use of external $H_2$ has a negative impact to the process. Direct dehydration of glycerol would form hydroxyacetone molecule without the need for hydrogen consumption

and under moderate conditions. Thus, the synthesis of 1,2-PDO from glycerol-derived hydroxyacetone offers a greener production method of 1,2-PDO and is one of the attractive paths for glycerol valorisation [3]. In addition, since hydroxyacetone is a highly reactive molecule, it can be used as an intermediate in organic synthesis to produce other compounds such as propionaldehyde, acetone and furan derivatives. Hydroxyacetone is a compound that lacks toxicity, which justifies its use in the textile, pharmaceutical and food industries. Furthermore , hydroxyacetone stands out as a key reagent for the production of lactic acid which has acquired significant interest since it is considered one of the 12 best molecules of the biological-based platform due to its wide potential applications in pharmaceutical and food industry or as biodegradable plastics among others [11].

Conventionally, hydroxyacetone has been synthesized by several ways: (i) reaction of bromoacetone with sodium or potassium formate (or acetate) followed by hydrolysis of the ester with methyl alcohol; (ii) direct oxidation of acetone with the Bayer-Villeger reagent [12]; (iii) dehydrogenation of aqueous propylene glycol in the presence of palladium-catalyzed hydrogen peroxide [13]; (iv) biosynthetic pathway which involves metabolically manipulated microorganisms using various substrates [14]. However, the presence of multi-step reagents in stoichiometric quantities, the low yields and the effluent disposal costs restrict the commercialization of any of these methods, thus the production of hydroxyacetone from inexpensive and often-wasted bio-glycerol is beneficial for environmental protection [9].

Sato *et al.* [15] investigated the dehydration of glycerol in the gas phase to hydroxyacetone over Ag catalysts achieving 91% conversion of glycerol with 86% selectivity to hydroxyacetone at 240°C under $H_2$ flow, however strong catalyst deactivation was observed. Chiu *et al.* [16] studied the conversion of glycerol in gas phase to hydroxyacetone in a high-pressure and high temperature semi-continuous reactor by reactive distillation over copper chromite catalyst. They observed 22% glycerol conversion and 70% hydroxyacetone selectivity. However, the toxicity associated to the Cr species in these catalysts and the deactivation due to coke formation requires further catalyst development. It has been reported that acidic sites have an important role in the glycerol dehydration and they can modulate the yield towards hydroxyacetone. The presence of Brönsted acid sites is reported to favor the dehydration of glycerol to acrolein, whereas Lewis acid sites promote the selective formation of hydroxyacetone [17].

Copper is recognized for its intrinsic ability to break preferentially the C-O primary bond of alcohols [18]. It is also suggested that copper oxide species act as Lewis acid sites to polarize the C-O bond of glycerol [19]. This property of copper is of vital importance for obtaining hydroxyacetone since this molecule is obtained by dehydration of any primary hydroxyl group of glycerol. The support material is known to participate directly on the selective dehydration. According to Sato *et al.* [1] the combination of an acid oxide support such as $Al_2O_3$ to copper effectively promotes the selectivity to hydroxyacetone in the glycerol conversion. This indicates that not only the copper species play an important role in the dehydration but the Lewis acid sites of the support are also important for the formation of hydroxyacetone. R. Mane *et al.* [9] investigated Cu-Al catalysts prepared by co-precipitation

and 24% glycerol conversion and 92% hydroxyacetone selectivity in the liquid phase were observed with an aqueous solution of 20 wt.% of glycerol, 220 °C and in a $N_2$ atmosphere.

In addition, P. Hirunsit *et al.* [20] have reported selectivity higher than 90% towards 1,2-PDO with copper catalysts supported on $Al_2O_3$. A. Bienholz *et al.* [21] reported for $Cu/SiO_2$ catalysts prepared by ammonia evaporation, 92% glycerol conversion and 69% selectivity to hydroxyacetone in gas phase with an aqueous solution of 40 wt.% glycerol in a $H_2$ atmosphere in a fixed bed reactor. It should be added that Dasari *et al.* [3] have reported that Raney copper has shown in the glycerol hydrogenolysis 69% selectivity towards 1,2-PDO with 49% conversion at 200°C and $H_2$ pressure of 14 atm.

The results outlined above may indicate that copper alone can catalyze glycerol dehydration and the support may facilitate copper species to be more active in the dehydration of glycerol. The present work focuses on the study of the selective dehydration of glycerol towards hydroxyacetone in aqueous phase on copper catalysts supported on materials with different nature of acid properties. Particularly in the present work it will be studied the effect of the total amount of acid sites; dispersion of copper species and the effect of three different supports ($SiO_2$, $\gamma$-$Al_2O_3$ and $ZrO_2$) in the selective dehydration of glycerol to hydroxyacetone.

## 2. Experimental

### *2.1 Catalyst preparation*

Cu/γ-$Al_2O_3$ and Cu/$ZrO_2$ catalysts were prepared by incipient impregnation with a 5% mass content of copper with respect to the weight of the support. The metal precursor was an aqueous solution of $Cu(NO_3)_2 \cdot 3H_2O$. After the impregnation step, the samples were kept under hood at room temperature for 4 hours and finally dried at 120 °C for 24 hours. Once dried they were calcined in a muffle with a heating ramp of 5 °C $min^{-1}$ from room temperature to 400 °C for 4 hours. Cu/$SiO_2$ catalyst was prepared by ammonia evaporation method [22] with a mass content of 5% of copper relative to the support. Briefly 25 wt.% ammonia solution was added in an aqueous solution of $Cu(NO_3)_2 \cdot 3H_2O$ under vigorous stirring until it reached pH 12. The resulting solution was heated to 80 °C maintaining this temperature until it reached a pH of 6.0-7.0. The final product was filtered and washed with water, followed by drying at 120 °C for 24 hours. It was then calcined in a muffle furnace with a heating ramp of 5°C $min^{-1}$ from room temperature to 400 °C for 4 hours. Finally, prior to the reaction the catalysts were reduced in a quartz reactor under $H_2$ flow at 50 mL $min^{-1}$ from room temperature to 400 °C with a heating ramp of 5 °C $min^{-1}$ and then they were kept at 400 °C for 4 hours.

### *2.2 Catalyst Characterization*

The specific surface areas of the copper-based catalysts were measured with a Micromeritics ASAP 2010 physisorption apparatus with $N_2$ at 77 K. BET and BJH methods were used respectively for the calculation of the surface areas and pore characteristics (size distribution

and volume). Prior to the analysis, the samples (about 100 mg) were degassed for 4 hours at 120 ° C using $N_2$ as a carrier gas.

X-ray powder diffraction (XRD) measurements were conducted on a Bruker X-ray diffractometer model D4 Endeavor (Kα Cu, 40 kV and 20 mA) operating with 2θ range of 20 - 90° at a scanning rate of 0.02° for 0.3 s.

FTIR spectra were collected using a FTIR-Vertex 70V instrument (Bruker) equipped with a Harrick cell TM (powder, ca. 30 mg). Prior to pyridine adsorption experiments, the samples were pre-treated at 400°C for 1 hour in hydrogen flow. The system was then cooled down to reach 150 °C under helium flow. Pyridine vapor adsorption was performed at 150 °C (30 spectra, 1 spectrum per minute). Finally, pyridine desorption was monitored for 1 hour under He flow at 150 °C from temperature ramping up (from 150 to 400 °C). Background spectra were collected before pyridine adsorption.

Temperature programmed desorption of $NH_3$ ($NH_3$-TPD) experiments were performed in a Micromeritics AutoChem II 2920 automatic equipment. Prior to the experiments, the catalysts (about 100 mg) were reduced at 400 °C for 120 min in 10% $H_2$/Ar at 20 mL $min^{-1}$, and after the reduction samples were cooled to 35 °C under the same flow. Then catalysts were treated with $NH_3$ (20 mL $min^{-1}$) for 10 min at 40 °C. Thus, the samples were treated in He flow (50 mL/min) to purge the system. Finally, the $NH_3$ desorption was carried out by heating the reactor with a temperature ramp of 5 °C $min^{-1}$ in a flow of He (20 mL $min^{-1}$). A trap of water, ice and NaCl salt was used. The $NH_3$ consumption has been determined by a thermal conductivity detector (TCD).

The amount of surface copper atoms was measured on the samples (about 100 mg) initially reduced in hydrogen flow of 50 mL $min^{-1}$ at 400 °C. The reduced samples were cooled in He flow (50 mL/min) to 60 °C and purged for 30 minutes. 20% $N_2O$/Ar gas was added for 1 hour. The selective oxidation of the copper surface to $Cu_2O$ was performed under 20% $N_2O$/Ar flow (50 mL $min^{-1}$) at 60 °C:

$$N_2O + 2Cu_{surface} \rightarrow Cu_2O_{surface} + N_2 \quad (1)$$

The system was then cooled to room temperature in He flow (50 mL $min^{-1}$) to eliminate the physisorbed species of $N_2O$. $Cu_2O_{surface}$ was further reduced with 5%$H_2$/Ar flow (50 mL $min^{-1}$) by raising the temperature at 5 °C $min^{-1}$ from room temperature to 900 °C. The $H_2$ consumption was followed by TCD detector.

$$H_2 + Cu_2O_{surface} \rightarrow 2Cu_{surface} + H_2O \quad (2)$$

VG Escalab 200R spectrometer equipped with a hemispherical electron analyser and an Mg Kα (hν=1253.6 eV, 1 eV=1.603 $\times 10^{-19}$ J) was employed for X-ray photoelectron spectroscopy (XPS) measurements. The X-ray source operated at 10 mA and 12 kV. The spectrometer chamber pressure during data acquisition was maintained at $1 \times 10^{-7}$ Pa. The peaks were fitted by a non-linear least square fitting program using a properly weighted sum of Lorentzian and Gaussian component curves after background subtraction. The constant charging of the samples was corrected by referencing all energies to the Al 2p peak at 74.5 eV.

*2.3 Catalytic Activity*

Dehydration of glycerol was studied in a 300 mL batch reactor with a content of 60 mL of reaction mixture with an aqueous solution of 80 wt.% of glycerol, 500 mg of catalyst which corresponds to a glycerol/Cu molar ratio of 1000. The reaction was carried out for 3 hours under a constant stirring of 800 rpm and temperature of 190 °C. The reaction was performed under $N_2$ atmosphere.

The reaction products were analysed at different reaction time by an autosystem XL gas chromatograph equipped with an FID detector and Nukol Capillary column (30 m long, 0.53 mm internal diameter and 0.5 μm film space) with He as a carrier gas. The products were also analysed with a gas chromatograph coupled to a mass spectrometer. The glycerol conversion and product selectivity were calculated according to:

$$Conversion\ (\%) = \frac{(moles\ of\ glycerol\ reacted)}{(initial\ \ moles\ of\ glycerol)} \times 100 \qquad (3)$$

$$Product\ i\ selectivity\ (\%) = \frac{(moles\ of\ C\ in\ the\ product\ i)}{(moles\ of\ C\ in\ the\ initial\ quantity\ of\ glycerol)} \times 100 \qquad (4)$$

To ensure the absence of intra-particle diffusion resistance the Weisz-Prater (WP) parameter was calculated. According to WP criteria, if WP ($\varphi$) ≤ 0.3 the internal diffusion resistance can be neglected for a heterogeneous reaction. Where $\varphi$ is:

$$\varphi = \frac{-r_{obs}\rho_c {R_p}^2}{D_e C_{AS}} \qquad (5)$$

Where, $-r_{obs}$ = the observed rate ($molg_{cat}^{-1}s^{-1}$), $\rho_c$ = solid catalyst density =2.08 $g.cm^{-3}$, $R_P$= catalyst particle radius = 0.0025 cm, $C_{AS}$ = concentration of glycerol at catalyst surface = 0,001 mol $cm^{-3}$. $D_e$ is the effective diffusivity of glycerol to water (2.11 x $10^{-5}$ $cm^2$ $s^{-1}$) and:

$$D_e = \frac{D_{AB}\phi\sigma}{\tau} \qquad (6)$$

Where $\phi$ = porosity pellet = 0.42, σ = constriction factor = 0.8 and τ = tortuosity = 3 [23, 24] and $D_{AB}$ = diffusion coefficient of glycerol to water at 250 °C = $1.85\times10^{-4}$ $cm^2s^{-1}$ calculated by Wilke-Chang Equation:

$$D_{AB} = \frac{1.173\times10^{-13}(\phi M_B)^{0.5}T}{\mu {V_A}^{0.6}} \qquad (7)$$

Where ϕ is the factor for solute-solvent interaction; Temperature (K); $V_A$ = molar volume of solute at boiling point (glycerol), $M_B$ = molecular weight of solvent (water) and $\mu$ is the solvent viscosity.

Finally $-r_{obs}$ is:

$$-r_{obs} = \frac{n}{V\times m_{cat}\times t} \qquad (8)$$

Where $n$ = moles of glycerol reacted, $V$ = volume in L, $m_{cat}$ = catalyst weight in g and $t$ = reaction time in minutes.

*2.4 Computational Details*

The Cu(111) surface model was constructed with a supercell of 4×4 containing 4 layers of metal atoms and a vacuum region ~15 Å. The two atomic layers from the bottom of the slab were fixed, while the top two layers were relaxed to their lowest energy configurations. The fixed layers were set to Cu bulk bond distances according to the optimized lattice constant

237 that was determined from bulk calculation. The slab model of γ-$Al_2O_3$(110) surface contains
238 thirty two $Al_2O_3$ molecular units and ~15 Å of the vacuum region. The (110) crystalline
239 surface was chosen because it dominates in γ-alumina nanocrystallites (~70-83% of total
240 area) [25, 26]. Twelve of $Al_2O_3$ molecular units located in atomic layers from bottom of the
241 slab were fixed and the rest were relaxed including the $Cu_{13}$ cluster and adsorbates. The fixed
242 layers were set to γ-$Al_2O_3$ bulk bond distances in which the γ-$Al_2O_3$ bulk model structure was
243 taken from references [25, 27]. The tetragonal $ZrO_2$ bulk structure was applied followed the
244 experimental observation. The slab model of most stable $ZrO_2$(111) surface was modeled
245 with total thirty nine molecular units and ~15 Å of the vacuum region excluding adsorbates.
246 Seventeen $ZrO_2$ molecular units from the bottom of a slab were fixed and the rest were
247 relaxed including $Cu_{13}$ cluster and adsorbates. The structures of bare Cu(111), $Cu_{13}$/γ-
248 $Al_2O_3$(110) and $Cu_{13}/ZrO_2$(111) are shown in Fig. S5 of supporting information.

249 The initial geometries of isolated $Cu_{13}$ cluster were modeled based on the possible $M_{13}$
250 nanoparticle structures reported in previous studies [28, 29]; icosahedral (ICO), face centered
251 cubic (FCC), hexagonal close packed (HCP), capped cubic (CC), buckled biplanar (BBP),
252 triangular biplanar (TBP), and cage-like (CAG). The two most stable structures of isolated
253 $Cu_{13}$ cluster structures were found to be ICO and BBP (Fig. S4 of supporting information).
254 Then, the optimized ICO and BBP $Cu_{13}$ clusters were initially placed on the γ-$Al_2O_3$(110)
255 and $ZrO_2$(111) surfaces with variations of location on the surfaces and orientations of the
256 $Cu_{13}$ clusters. The most stable structures found for $Cu_{13}/Al_2O_3$(110) and $Cu_{13}/ZrO_2$(111) (Fig.
257 S5 of supporting information) were then applied for glycerol and hydroxyacetone adsorption
258 study. The 13-atom Cu cluster model can represent small particle size (~ 1nm) which has an
259 average number of metal atoms in the range 11-14 atoms. The models present Cu-Cu and

Cu-support interaction. $Cu_{13}$ cluster were widely applied to study catalytic reaction such as CO oxidation and ammonia decomposition [30-32]. It should be noted that the copper particle size and shape can affect the reactivity as well which may be due to the variation of the amount of low coordinated defect sites. The supported metal-13 cluster on support such as γ-$Al_2O_3$ surface also were previously employed to study NO oxidation [33], $H_2$ dissociation [34], the nature of the metal-support interaction [35], and stability of clusters on support [36].

Hydroxyl are created and adsorbed on $Al_2O_3$ and $ZrO_2$ surfaces due to the adsorption of water which is a product of glycerol dehydration [25, 37]. The effect of hydroxylation on the supports were also investigated. The relationship between the hydroxyl coverage on γ-$Al_2O_3$(110) surface and temperature has been investigated previously by Digne *et al.*[25] Applying this relationship, the OH coverage on γ-$Al_2O_3$(110) surface corresponding to the experimental temperature in the range of 130-230 $^oC$ is approximately 3.0-11.8 OH $nm^{-2}$. The approximately 4.5 OH $nm^{-2}$ coverage corresponding to 4 $H_2O$ molecules on the γ-$Al_2O_3$(110) and $ZrO_2$(111) surfaces were employed in this work. The hydroxyl group adsorption was particularly located nearby the copper cluster model in order to bring in the effect of hydroxylation on the dual roles of support and copper cluster.

The Vienna *ab initio* Simulation Program [38, 39] was employed to perform fully periodic plane-wave density functional theory (DFT) calculations. Spin-polarized DFT calculations were performed using the GGA-PBE functional [40] implemented with the Projector Augmented Wavefuction (PAW) [41, 42] method for representing the non-valence core electrons. The long-range dispersion force was included using the semi empirical dispersion potential correction method described by Grimme and coworkers [43, 44]. The plane-wave energy cutoff was optimized at 450 eV. The Gaussian broadening [45] with a smearing width

of 0.1 eV was employed. The dipole correction was included only in z direction and the surface Brillouin zone was sampled with a 2×2×1 Monkhorst-Pack k-point mesh [46] for all surface calculations. The results were checked for convergence with respect to energy cutoff and number of k-points. The convergence criterion for electronic self-consistent iteration was set to $10^{-7}$ eV and the ionic relaxation loop was limited for all forces smaller than 0.030 eV $Å^{-1}$ for free atoms. Bader charge analysis was performed using VASP-VTST [47–49].

## 3. Results

### *3.1 Catalyst characterization*

The textural properties of the supports and copper catalysts are summarized in Table 1 and Fig. 1. Specific area ($S_{BET}$), pore volume ($V_{pore}$) and pore diameter ($d_{pore}$) of the catalysts decrease compared to their supports due to the introduction of copper, indicating a partial blockage of the pores. $ZrO_2$ and $SiO_2$ exhibited the smallest and the highest specific surface area, respectively.

Table 1. Textural parameters of supports and copper catalysts.

| Sample | $S_{BET}$ ($m^2\ g^{-1}$) | $V_{Pore}$ ($cm^3\ g^{-1}$) | $d_{pore}$ (nm) |
|---|---|---|---|
| $ZrO_2$ | 146 | 0.17 | 4.3 |
| $\gamma$-$Al_2O_3$ | 212 | 0.39 | 7.4 |
| $SiO_2$ | 319 | 0.85 | 10.6 |
| 5% Cu/$ZrO_2$ | 131 | 0.13 | 4.0 |
| 5% Cu/$\gamma$-$Al_2O_3$ | 181 | 0.34 | 7.5 |
| 5% Cu/$SiO_2$ | 244 | 0.70 | 11.6 |

Fig. 1a shows $N_2$ sorption isotherms of the supports and Cu catalysts. Isotherms displayed a type-IV curves characteristic of mesoporous structure [50]. For $SiO_2$-based materials a H1-type hysteresis loop corresponding to uniform spherical pores from a regular matrix of pore size distribution centered at 10-12 nm (Fig. 1b) was found. For materials based on $\gamma$-$Al_2O_3$ and $ZrO_2$ a H2-type hysteresis loop and pore size distribution centered at 4 and 7 nm were found, respectively.

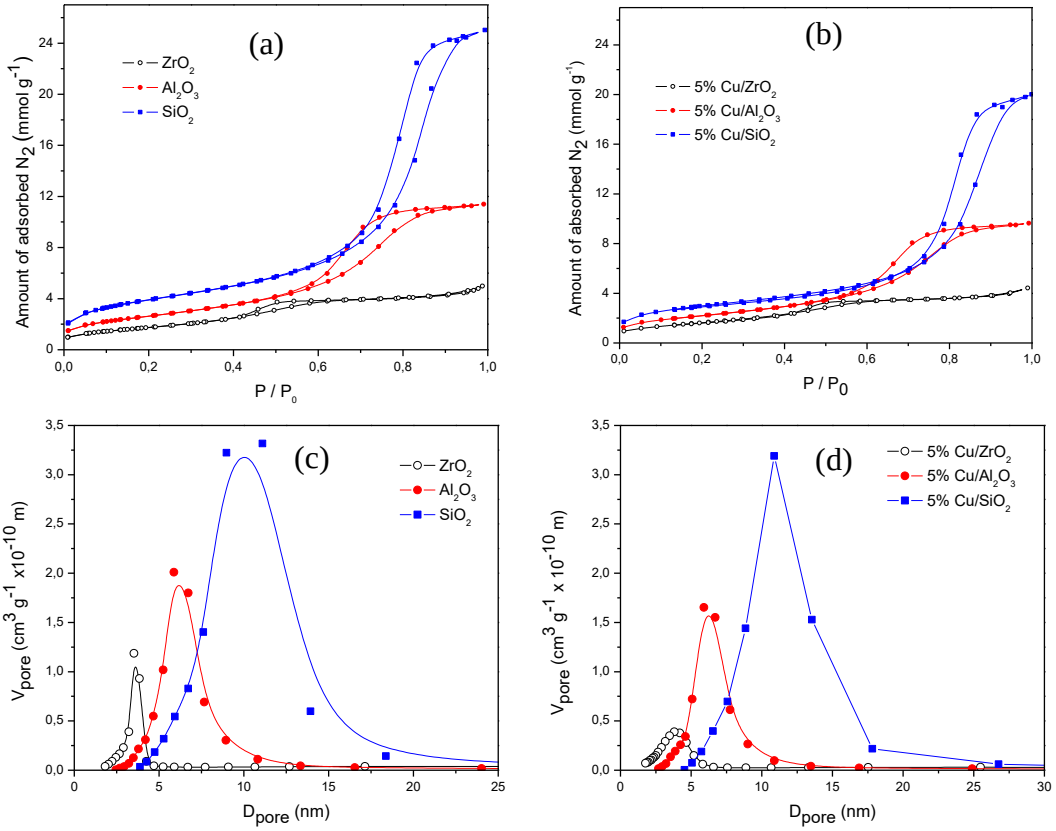


Fig. 1. (a) and (b) $N_2$ adsorption-desorption at 77 K and (c) and (d) Pore size distribution.

By XRD, diffraction peaks only due to the support materials (Fig. 2) were found for all samples. Copper species are expected to exhibit reflection peaks as follows: metallic copper ($Cu^0$) at $2\theta$ = 43, 50 and 74 ° (JCPDS 04-0836), copper (II) oxide (CuO) at $2\theta$ = 32.6, 35.6,

38.6, 48.8, 53.6, 58.3, 61.6, 66.4, 68.1, 72.3 and 75.1 ° (JCPDS 48-1548) and copper (I) oxide (cuprous oxide, $Cu_2O$) at 2θ = 36.4, 42.3 and 61.3 ° (JCPDS 05-0667). The absence of the reflection peaks due to copper species indicates their high dispersion. At 7 wt.% of copper it is reported to be possible to identify Cu peaks in the XRD analysis [51]. Previous work reported that the highly crystalline CuO is formed from approximately 4 wt.% of Cu for 100 $m^2 g^{-1}$ of γ-$Al_2O_3$ [52].

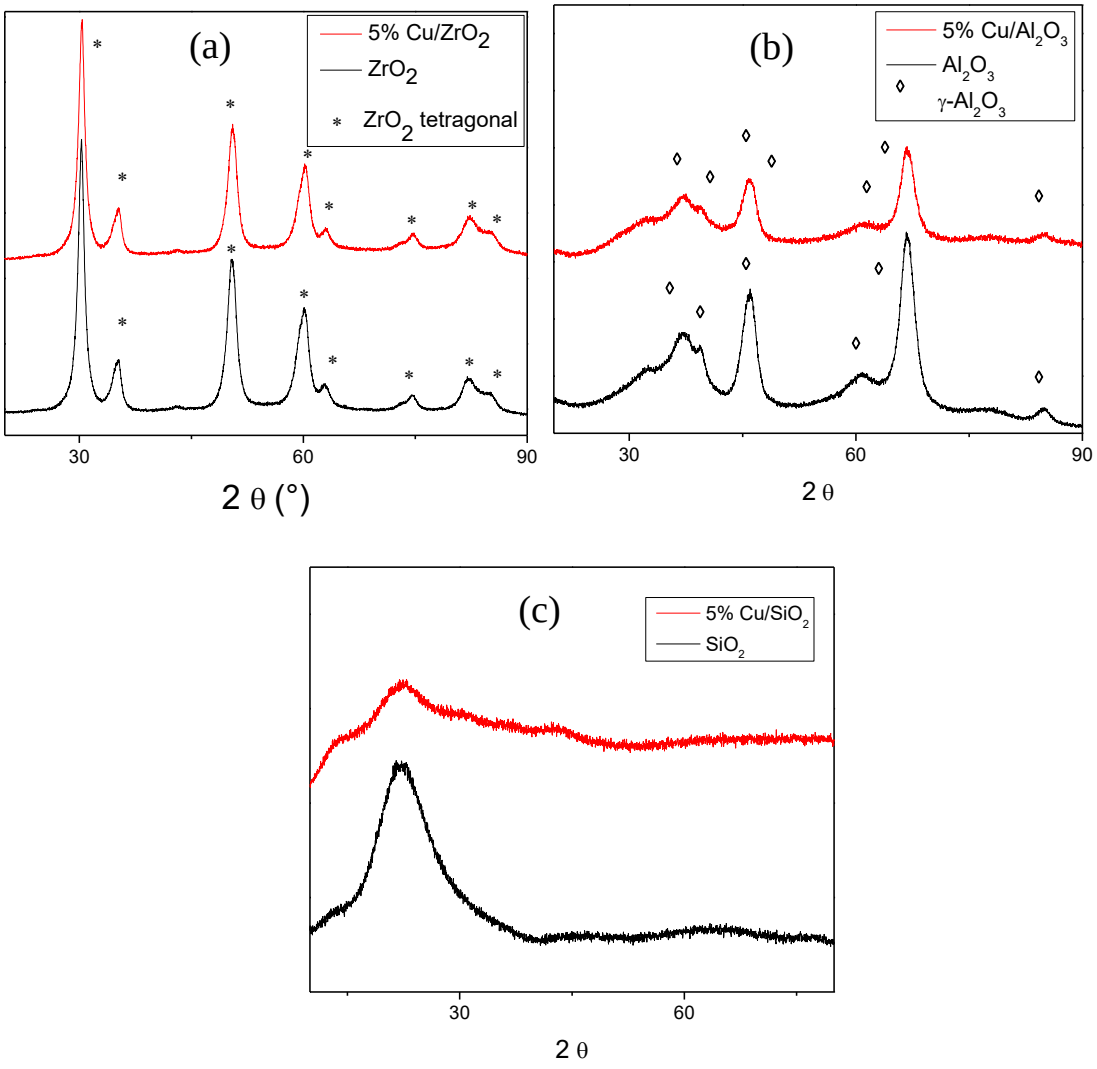


Fig. 2. Powder XRD patterns of (a) $ZrO_2$ (b) γ-$Al_2O_3$ and (c) $SiO_2$ materials.

Only tetragonal zirconia (no monoclinic) patterns were observed in $ZrO_2$-based materials (Table 2). For the materials based on γ-$Al_2O_3$ the presence of characteristic peaks of the support (JCPDS 029-0063) was observed at 2θ = 31.9, 37.6, 39.5, 45.8, and 66.7°. X-ray diffraction reveals the amorphous nature of $SiO_2$.

Table 2. XRD pattern of monoclinic (JCPDS 37-1484) and tetragonal $ZrO_2$ (JCPDS 17-0923).

| Monoclinic $ZrO_2$ | | Tetragonal $ZrO_2$ | |
|---|---|---|---|
| 2θ (°) | Crystallographic plane | 2θ (°) | Crystallographic plane |
| 24.2 | (0,1,1) | 30.1 | (1,1,1) |
| 28.2 | (1,1,0) | 35.2 | (2,0,0) |
| 31.4 | (0,2,0) | 50.4 | (2,2,0) |
| 34.3 | (1,2,1) | 59.9 | (3,1,1) |

The evaluation of acidity of the support and catalyst materials by $NH_3$-TPD (Table 3 and Fig. 3) showed an increase of the total acidity for the catalysts containing copper species. $Cu/ZrO_2$ has the highest acidity (867 μmol $g_{cat}^{-1}$) in contrast to $Cu/SiO_2$ that presented the lowest total amount of acid sites (187 μmol $g_{cat}^{-1}$).

Table 3. Quantitative analysis of $NH_3$-TPD data of $ZrO_2$, γ-$Al_2O_3$ and Cu-based catalysts.

| Sample | Total $NH_3$ amount | |
|---|---|---|
| | (μmol $g_{cat}^{-1}$) | (μmol $m^{-2}$) |
| $ZrO_2$ | 360 | ----- |
| γ-$Al_2O_3$ | 280 | ----- |
| 5% $Cu/ZrO_2$ | 867 | 6.6 |
| 5% $Cu/Al_2O_3$ | 591 | 3.3 |
| 5% $Cu/SiO_2$ | 187 | 0.8 |

$ZrO_2$ support showed a signal with a maximum at 270 °C and a tail-like broad desorption extending to approximately 630 °C, indicating a wide distribution of the strength of the acid sites ranging from moderate (considered from 200-450 °C) to strong (> 450 °C) ones. The $Cu/ZrO_2$ catalyst also exhibited a wide distribution of acid sites with different acid strengths and the total amount of acid sites that increases with the introduction of copper species. This could be attributed to the contribution of copper oxide species. Similarly, a heterogeneous distribution of acid sites for the $\gamma$-$Al_2O_3$ system is highlighted. A minor or negligible total amount of acid sites in the $SiO_2$ support was found.

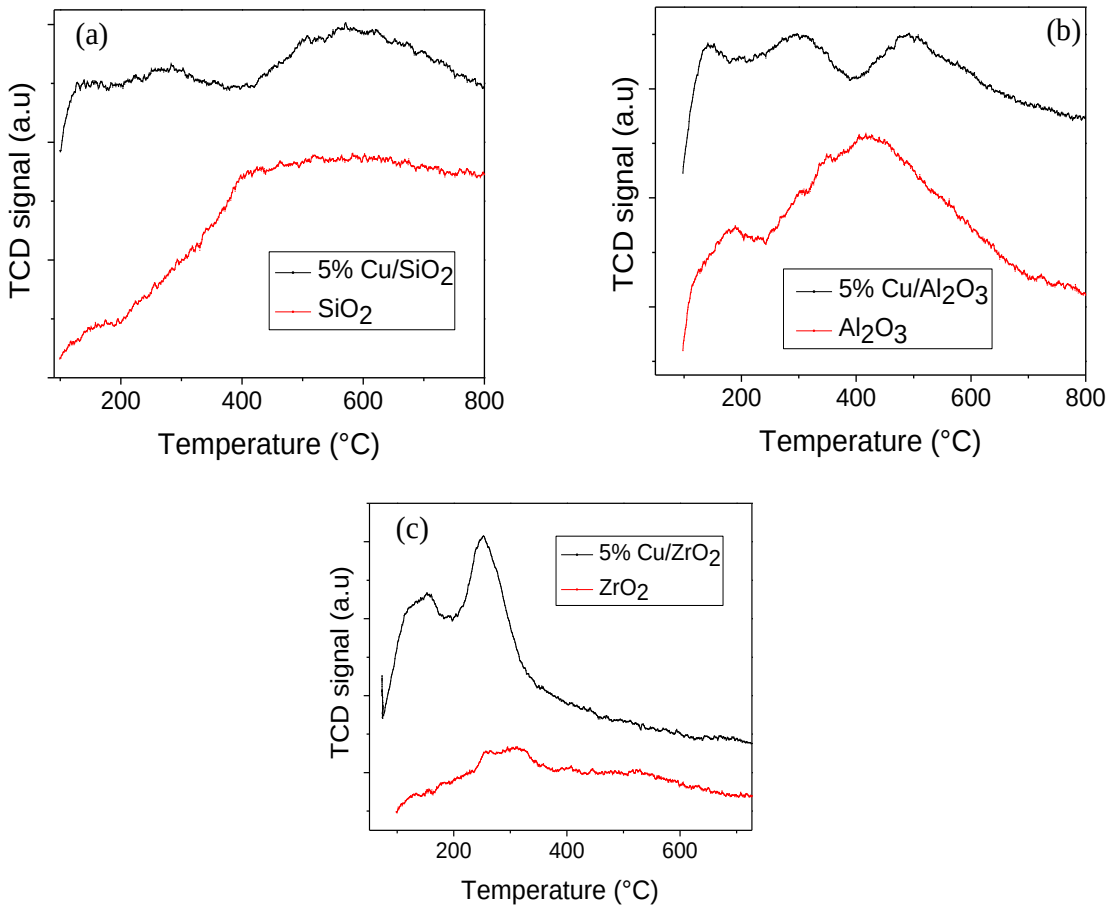

Fig. 3. Temperature-programmed desorption of ammonia profiles of supports and Cu-based catalysts (a) $SiO_2$ and 5%Cu/$SiO_2$, (b) $Al_2O_3$ and 5%Cu/$Al_2O_3$ and (c) $ZrO_2$ and 5%Cu/$ZrO_2$.

Brönsted and Lewis acidity were identified by FTIR of pyridine as shown Fig. 4. The IR spectra of the support materials and supported copper catalysts were compared in the region of 1600-1400 $cm^{-1}$. From the IR spectra only Lewis acid sites were identified over the support materials. The IR spectra of the supports ($\gamma$-$Al_2O_3$ and $ZrO_2$) show bands at about 1455, 1490 and 1610 $cm^{-1}$ after pyridine desorption at 400 °C. The band observed at 1455 $cm^{-1}$ is attributed to the presence of hydrogen-bonded pyridine adsorbed on Lewis acid sites [53]. The observed band at 1610 $cm^{-1}$ is ascribed to pyridine strongly bound on Lewis acid sites [54]. The band observed at about 1490 $cm^{-1}$ is attributed to pyridine adsorbed on both Lewis and Brönsted acid sites. There is no evidence for a band at about 1610 $cm^{-1}$ (Fig. 4) in the infrared spectra of pyridine desorption on $SiO_2$. In addition, there is no evidence for a band at 1540 $cm^{-1}$ suggesting no Brönsted acidity for $SiO_2$ sample in agreement with literature [55]. It must be added that the absence of the band at 1490 $cm^{-1}$ suggests negligible Lewis acidity in $SiO_2$ support.

Supported copper catalysts were reduced at 400 °C in hydrogen prior the pyridine measurements. Impregnation of copper on $ZrO_2$, $\gamma$-$Al_2O_3$ and $SiO_2$ resulted in the appearance of Lewis and Brönsted acid sites. The bands corresponding to Brönsted acid sites were observed at 1548 $cm^{-1}$ for copper supported on $\gamma$-$Al_2O_3$ and $ZrO_2$ [56]. In contrast, Cu/$SiO_2$ catalyst exhibited only Lewis acid sites.

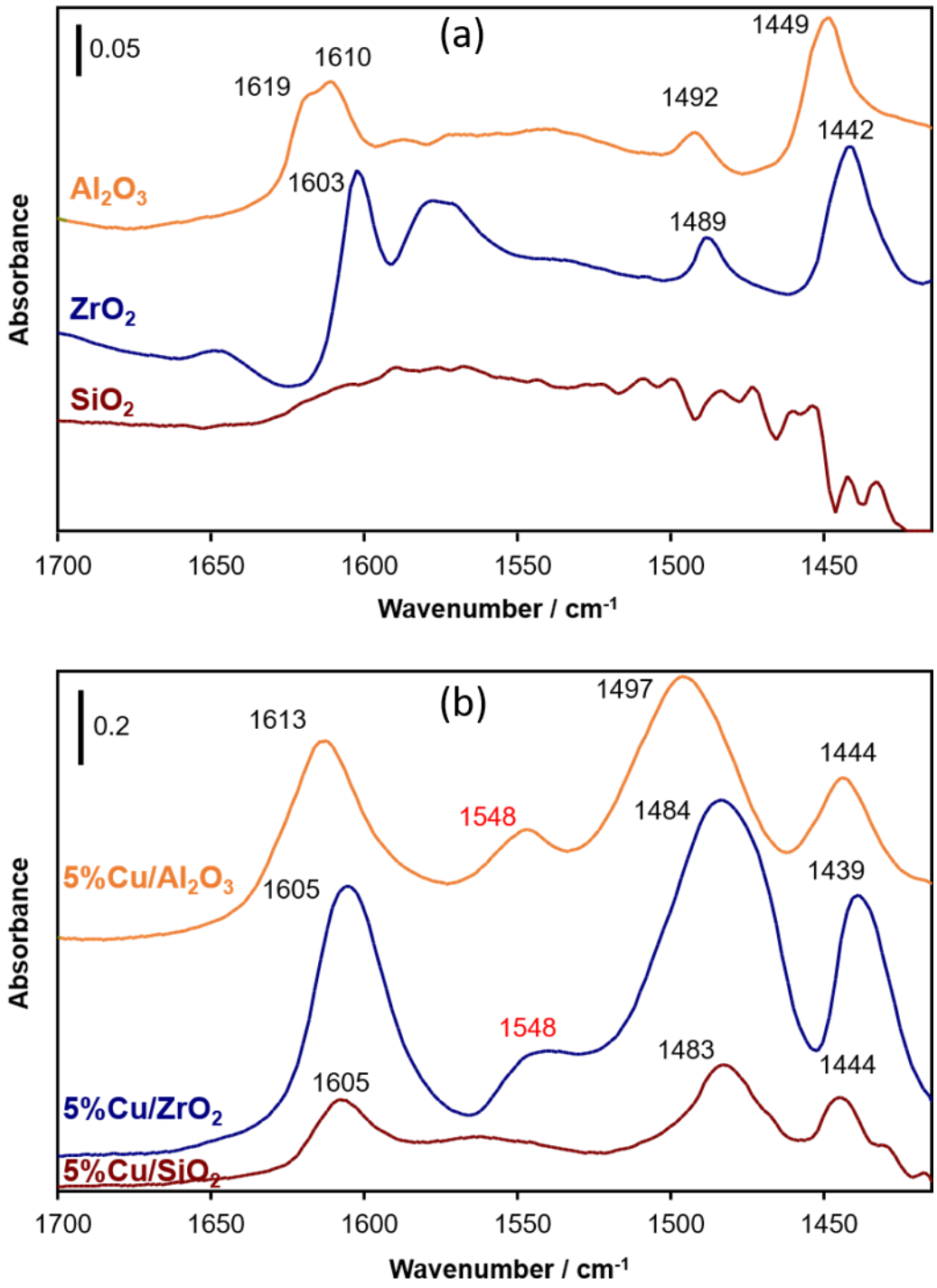


374

375 Fig. 4. FTIR of (a) supports and (b) catalyst after pyridine desorption at 400 °C.

376

TPR profiles of the calcined copper catalysts at 400 °C are shown in Fig. 5. $Cu/SiO_2$ catalyst exhibits a nearly symmetrical reduction peak at ca. 200 °C. For $Cu/Al_2O_3$ catalyst, the main reduction peak is also centred at ca. 200 °C. It is observed that the catalysts $Cu/SiO_2$ and $Cu/Al_2O_3$ have an reductive event at the same temperature which suggests a homogeneous copper species distribution and the corresponding reduction refers to $Cu^{+2} \rightarrow Cu^0$ [57].

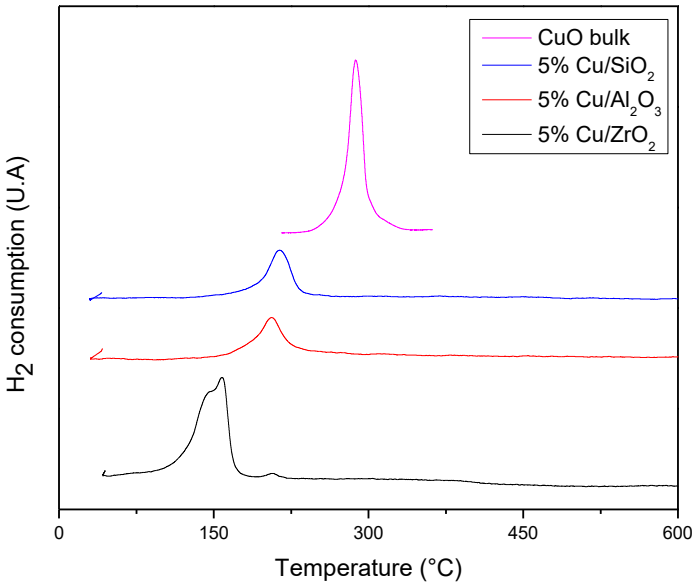


Fig. 5. TPR of copper based catalysts.

For $Cu/ZrO_2$ sample the main reduction peak shifts to lower temperature at ca. 160°C and presents a shoulder peak at ca. 140°C. Liu *et al.* [58] observed two overlapping peaks with apparent maxima at 140°C and 160°C for the reduction of copper supported on tetragonal zirconia. According to these authors, these peaks correspond to highly disperse $Cu^{+2}$ species assigning the first peak to the reduction of $Cu^{+2} \rightarrow Cu^{+1}$, followed by a second event to $Cu^{+1} \rightarrow Cu°$. The reduction profile of $Cu/ZrO_2$ sample suggests a strong influence of the support

400 on the reduction of copper species. A shift towards lower temperatures with respect to the
401 other two supports ($\gamma$-$Al_2O_3$ and $SiO_2$) is observed. This is attributed to promoter effects of
402 $ZrO_2$ in the reducibility of copper species. It must be added that only a minor reduction peak
403 at $200^0$C was visible for Cu/$ZrO_2$. This peak can be attributed to the reduction of bulk CuO
404 [59]. The low reduction temperature strongly suggests the presence of finely dispersed copper
405 species embedded homogeneously in the $ZrO_2$ support. The higher reduction temperature
406 peak is assigned to the reduction of CuO crystallites [60].
407
408 The existence of vacancies on the surface of the support is a vital factor in achieving
409 dispersion of ionic species [61]. $Cu^{+2}$ species can be located at surface vacancies of $ZrO_2$
410 leading to a high dispersion of copper. These species are responsible for the low temperature
411 reduction peaks. Previous work reports a dispersion capacity of 8.6 ions of $Cu^{+2}$ per $nm^2$ of
412 $ZrO_2$. Loads of copper species higher than this dispersion capacity of $ZrO_2$ will result in the
413 formation of $Cu^{+2}$ ions being gradually surrounded by other $Cu^{+2}$ ions forming CuO bulk
414 species leading to an increase of the reduction temperature of these species [58]. Bulk CuO
415 exhibits a broad TPR peak at ca. 300°C (Fig. 5).
416
417 $\gamma$-$Al_2O_3$ is also able to stabilize $Cu^{+2}$ due to the existence of tetrahedral and octahedral
418 vacancies on its surface [62], while $SiO_2$ is not able due to its structurally saturated surface.
419 Previous work [63] reported the formation of bulk CuO modulated in terms of the ratio
420 Cu/SSA or "copper charge/specific support area (SSA)" of 4.5 atoms of Cu per $nm^2$ of $ZrO_2$
421 support. Considering that the $ZrO_2$ used in our work has a specific surface area of 146 $m^2$ $g^{-1}$
422 the appearance of bulk CuO would occur approximately in copper charges of 7 wt.%. In

addition, considering that the γ-$Al_2O_3$ used in our work has a specific surface area of 212 $m^2$ $g^{-1}$ it can be expected that the formation of CuO species would begin to appear with copper loading close to 10 wt.%. The detection of CuO bulk species in the XRD profiles (Fig. 2) is somewhat difficult.

Dispersion on metallic copper and the specific copper surfaces of the catalysts were determined by chemisorption of $N_2O$. Cu/$ZrO_2$ shows the highest dispersion with 38% and the largest metallic surface area of Cu° (Table 4). Although $ZrO_2$ has the smallest specific surface it is able to disperse substantial amount of impregnated copper species due to the strong interaction between copper species and support [64]. Cu/$SiO_2$ shows a significantly lower copper dispersion and specific copper surface of the catalysts which are more likely due to a more intense sintering of copper particles.

Table 4. Catalysts characterization by $N_2O$ chemisorption

| Parameter \ Catalyst | 5%Cu/$SiO_2$ | 5%Cu/γ-$Al_2O_3$ | 5%Cu/$ZrO_2$ |
|---|---|---|---|
| $N_2O$ (μmol $N_2O$ $g_{cat}^{-1}$) | 203 | 277 | 301 |
| Dispersion (%) | 26 | 35 | 38 |

XPS parameters from the reduced copper catalysts are summarized in Table 5 and Fig. 6.

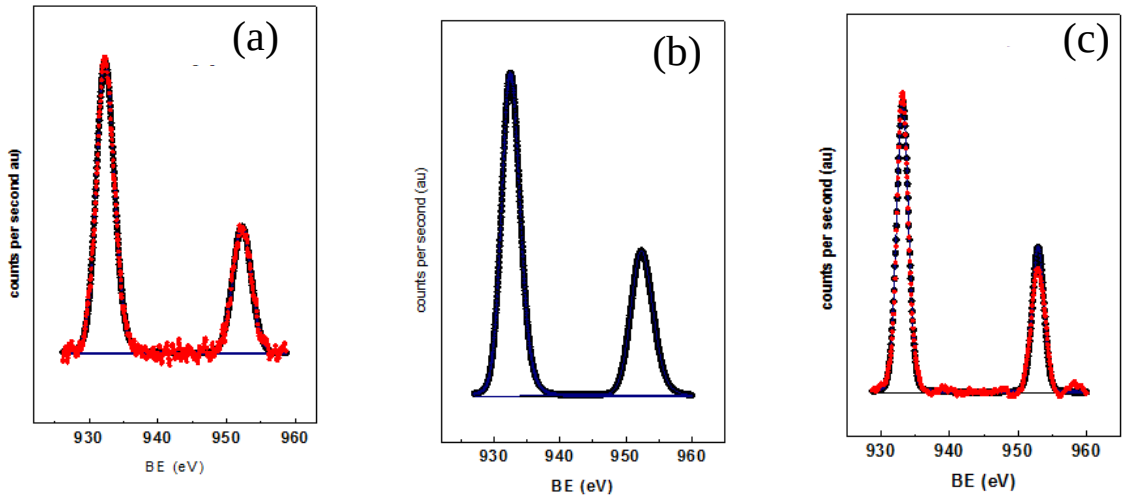


439 Fig. 6. XPS of (a) 5%Cu/$SiO_2$, (b) 5%Cu/$Al_2O_3$ and (c) 5%Cu/$ZrO_2$.

440

441 All reduced catalysts exhibited symmetrical $Cu3p_{3/2}$ and $Cu2p_{1/2}$ peaks with binding energies
442 between 932.5 and 952.4 eV respectively. A satellite was not detected at approximately 942
443 eV suggesting absence of $Cu^{+2}$ species [65]. Because the binding energies of Cu° and $Cu^{+}$
444 are similar it is difficult to differentiate them based only on $Cu3p_{3/2}$, so we used the modified
445 Auger parameter (αCu) for further conclusions.

446

447 Table 5. Binding energies (eV) of internal levels, Auger parameter and atomic ratios of
448 supported copper catalysts

| Catalyst | $Cu2p_{3/2}$ | M2p or M3d | αCu (Auger) | Cu/M[a] atomic ratio |
|---|---|---|---|---|
| 5%Cu/$ZrO_2$ | 932.5 | 182.2 | 1850.9 | 0.016 |
| 5%Cu/$Al_2O_3$ | 932.5 | 74.5 | 1851.0 | 0.021 |
| 5%Cu/$SiO_2$ | 932.4 | 103.4 | 1850.8 | 0.027 |

449

450 The value of αCu at approximately 1851.0 eV for reduced copper catalysts suggests that the
451 copper species may prevail on the catalyst surface as Cu°. The value of the atomic surface
452 ratio Cu/M (M=Al, Si, Zr) determined via XPS for the reduced samples increases in the
453 following order: $Cu/ZrO_2$ < $Cu/\gamma$-$Al_2O_3$ < $Cu/SiO_2$. The difference in the distribution of
454 copper species on each support can be tentatively identified with the Cu/M surface atomic
455 ratio value. In this case, a lower Cu/M suggests a more homogeneous distribution of copper
456 species on $ZrO_2$ support in agreement with the aforementioned results via XRD (Fig. 2), TPR
457 (Fig. 5), chemisorption of $N_2O$ (Table 4).
458
459 *3.2 Catalytic activity*
460 Glycerol conversion profile in the first 120 minutes of reaction was used to determine the
461 kinetic parameters such as the reaction order (*n*) and the apparent kinetic constant (*k*) values
462 expressed in terms of $min^{-1}$ $m_{cat}^{-2}$. The first 120 minutes have been studied in order to ensure
463 the evaluation of the catalytic performance under conditions where the reaction is kinetically
464 controlled and there is a minimization of the influence of possible product-catalyst
465 interaction. Moreover, for the determination of the kinetic constant an isothermal process;
466 constant volume of the reaction medium and absence of mass transfer effect have been
467 considered. The Weisz-Prater (WP) criterion was used to verify the absence of intraparticle
468 diffusion limitation as well as the assumption of spherical particles and the consideration of
469 an apparent first order reaction. It was obtained a value of WP of 0.12 in the worst scenario.
470 WP values less than 0.3 ensure that there is no mass transfer, thus our system meets the WP
471 criteria. After 2 hours of reaction the conversion observed for 5%$Cu/ZrO_2$, 5%$Cu/Al_2O_3$ and
472 5%$Cu/SiO_2$ catalysts were at about 30%, 25% and 22%, respectively.

473 In the present study the activity results were expressed in terms of conversion (*X*). The same
474 catalytic test was performed multiple times to check the reproducibility. The results are
475 presented in Fig. 7 with the plot of *–ln(1-X)* versus *time* to demonstrate an apparent kinetic
476 of an irreversible first order reaction with a constant density system. A straight line passing
477 through the origin was obtained (Fig. 7) where the corresponding slope is equal to the
478 apparent kinetic constant of each catalyst. It was represented the results from the repeated
479 experiments for each catalyst in the corresponding plot. The highest kinetic constant was
480 found for the 5%Cu/$ZrO_2$ catalyst.
481

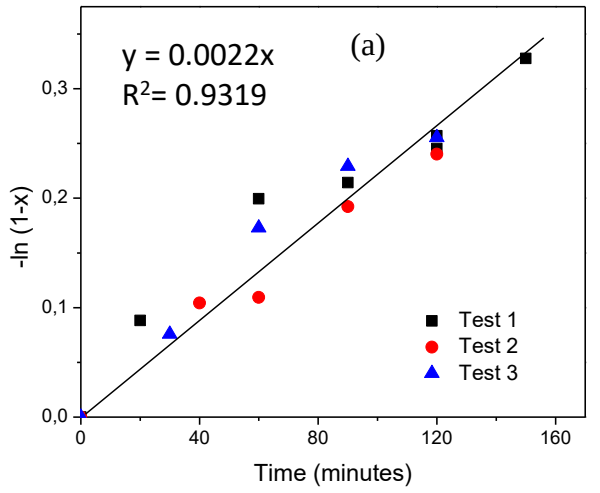

482

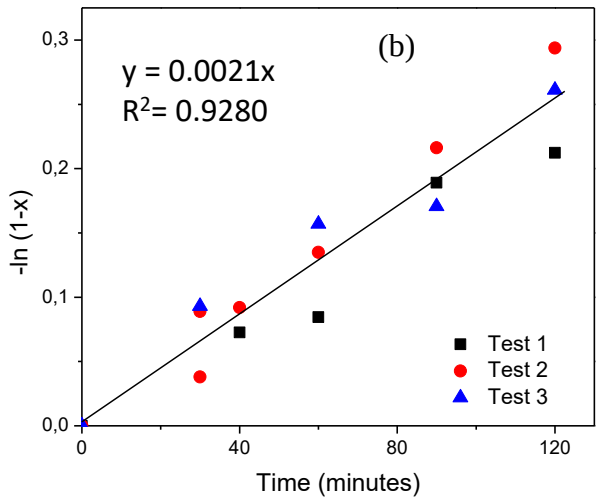

483

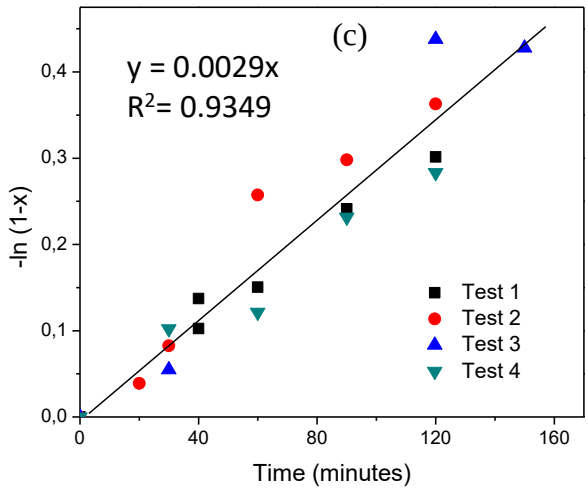


Fig. 7. Reaction demonstrating an apparent first order kinetic (a) 5%Cu/$SiO_2$, (b) 5%Cu/$Al_2O_3$ and (c) 5%Cu/$ZrO_2$.

The physical-chemical properties of the support have vital influence on the dispersion of metallic copper species influencing the catalytic performance as noticed in Table 6, which represents the relationship of the kinetic constants expressed in μmol $m_{cat}^{-2}$ with the total quantity of $N_2O$ chemisorbed (μmol $m_{cat}^{-2}$). Table 6 also shows the relationship of the corresponding kinetic constants to the total acidic sites expressed in (μmol $m_{cat}^{-2}$). Thus, an increase in the apparent kinetic constant with both total quantity of $N_2O$ chemisorbed and the total quantity of acidic sites was observed.

Table 6. Apparent kinetic constant of the copper catalysts

| Apparent first order kinetic constant, k | 5%Cu/$SiO_2$ | 5%Cu/γ-$Al_2O_3$ | 5%Cu/$ZrO_2$ |
|---|---|---|---|
| k ($min^{-1}$) | 0.0022 | 0.0021 | 0.0029 |
| k ($min^{-1}$ $m_{cat}^{-2}$) | $4.5\times10^{-6}$ | $5.8\times10^{-6}$ | $1.1\times10^{-5}$ |

Under the experimental conditions, a negligible conversion of glycerol and hydroxyacetone selectivity were observed when the supports were directly used as catalysts in the activity tests. Fig. 8 shows their catalytic performance monitored in different times of reaction. $Cu/ZrO_2$ catalyst (Fig. 8a) shows a glycerol conversion of at about 4% at 20 minutes reaching at about 30% of conversion at 120 minutes of reaction. $Cu/\gamma\text{-}Al_2O_3$ (Fig. 8b) exhibits a glycerol conversion between 8 to 25% in the range of 120 minutes of reaction. In the case of $Cu/SiO_2$ catalyst (Fig. 8c) it is observed a glycerol conversion of 8% at 20 minutes of reaction and at about 20% of conversion at 120 minutes of reaction.

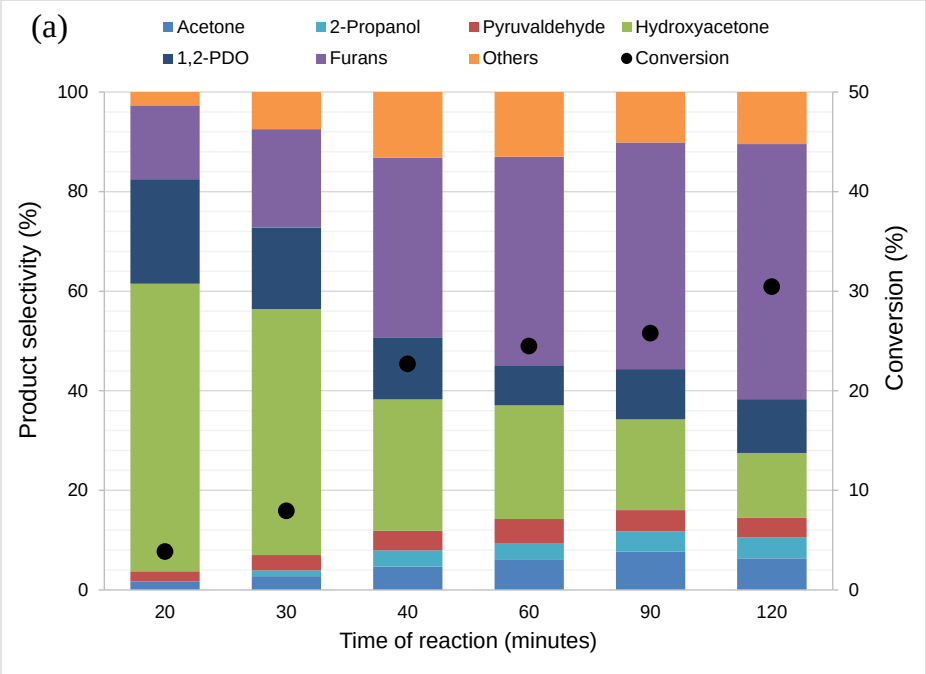

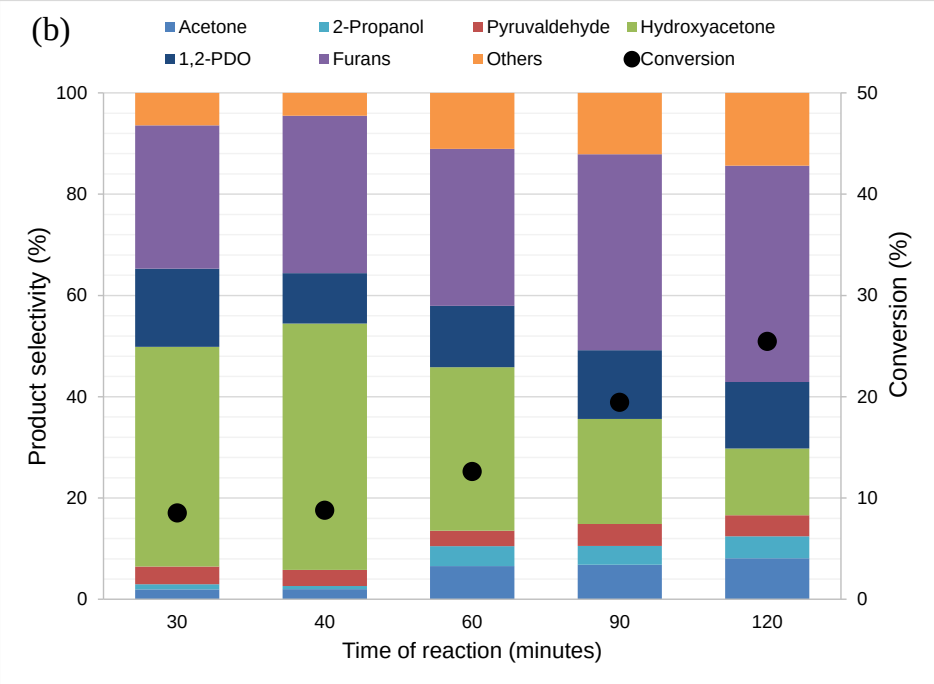


510

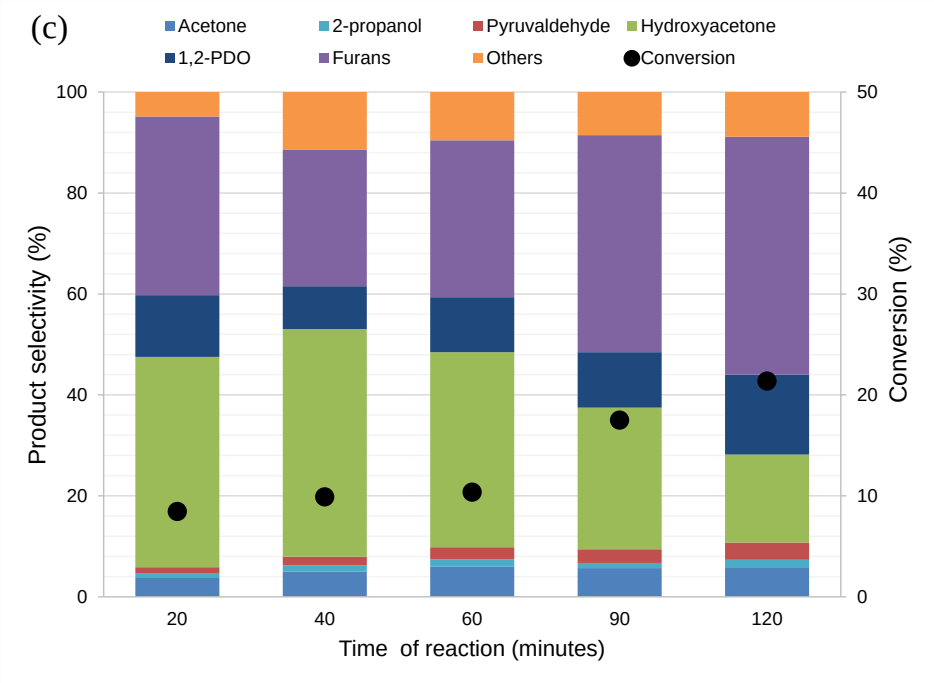


511

512 Figure 8. Catalytic performance of copper based catalysts. (a) 5%Cu/$ZrO_2$, (b) 5%Cu/$Al_2O_3$

513 and (c) 5%Cu/$SiO_2$.

514

The main products observed in the reaction was acetone, 2-propanol, pyruvaldehyde, hydroxyacetone, 1,2-propanediol, furan derivatives and other unidentified compounds possibly produced by secondary reactions between the compounds in the reaction mixture. It is noticed for the copper catalysts that the highest selectivity towards hydroxyacetone was in first minutes of reaction. In this respect, hydroxyacetone selectivity of 57% and 41% was observed respectively for $Cu/ZrO_2$ and $Cu/SiO_2$ catalysts at 20 minutes of reaction, whereas for $Cu/\gamma\text{-}Al_2O_3$ sample a hydroxyacetone selectivity of 43% was noticed at 30 minutes of reaction. Previous work [9] reported over Cu-Al (50:50) catalyst prepared by coprecipitation a hydroxyacetone selectivity of 92% and 24% of glycerol conversion at 493 K in aqueous medium under $N_2$ atmosphere in autogenous condition. W. Suprun *et al.* [66] reported hydroxyacetone selectivity of 23% and 100% of conversion in the dehydration of glycerol over $Al_2O_3\text{-}PO_4$ catalyst at $280^0$C. Chiu et al.[16] reported that copper-chromite catalyzes the dehydration of glycerol with a selectivity towards hydroxyacetone of 70% and 22% of glycerol conversion.

Hydroxyacetone was the major product observed in the initial reaction period as shown Fig. 9. In addition, the highest yield towards hydroxyacetone was noticed for $5\%Cu/ZrO_2$. Hydroxyl terminal groups of the glycerol molecule interacting with the Lewis acid sites on the catalyst surface may promote the formation of an enol intermediate which rapidly reorganizes to form hydroxyacetone. Thus, hydroxyacetone can be obtained by direct dehydration of glycerol followed by a keto-enolic tautomerization [67]. Pyruvaldehyde was also observed and it can be formed from hydroxyacetone dehydrogenation.

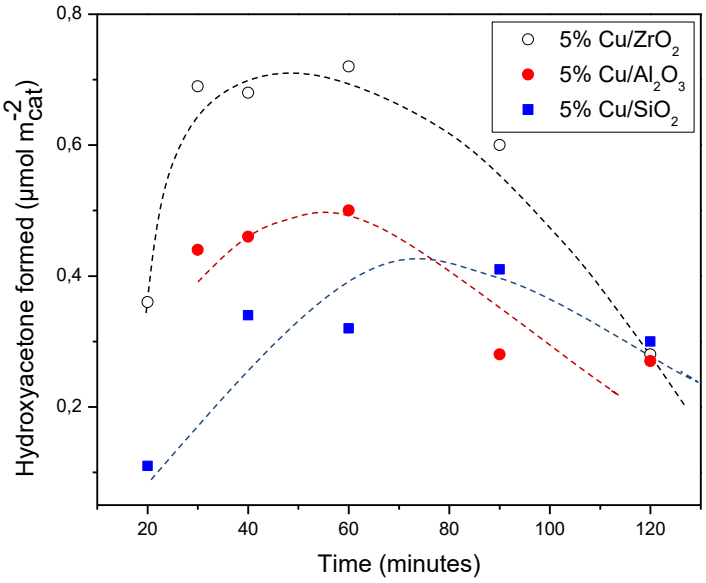


Fig. 9. Glycerol conversion towards hydroxyacetone. (Dashed lines only serve to guide the eyes).

After 120 minutes of reaction, acetone, 2-propanol and furan derivatives were also observed. These products were formed from the degradation of hydroxyacetone. Earlier works report that hydroxyacetone is converted to carboxylic acids which allow acetone to be formed via ketonization. Catalytic cyclisation to form furan derivatives are also observed. It must be added that 1,2 propanediol (1,2-PDO) was also detected. Previous work [9] reported that glycerol hydrogenolysis to 1,2-PDO proceeds through a dehydrogenation-dehydration-hydrogenation mechanism. In that case hydroxyacetone is the intermediate to 1,2-PDO. Copper may serve as active sites for the subsequent hydrogenation step to 1,2-PDO by the formation of active hydrogen atom originating from the dehydrogenation step. The general chemical route based on the main products detected by gas chromatograph and mass spectrometry is shown in Scheme 1.

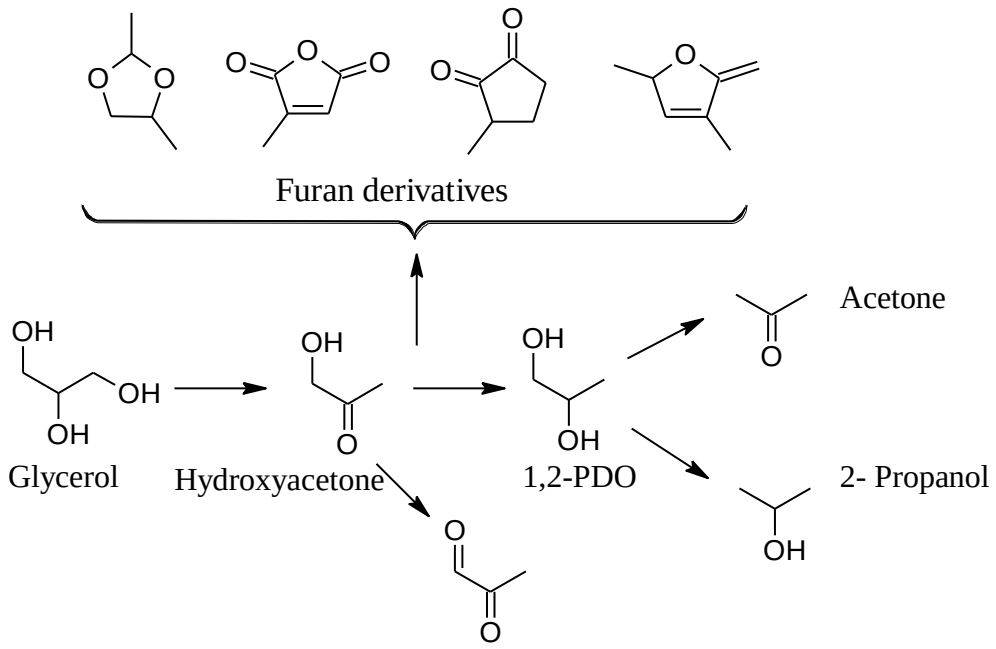


Scheme 1. Identified products in the glycerol dehydration.

*3.3 Catalyst Recycling*

The recycling of 5%Cu/$ZrO_2$ catalyst during the selective conversion of glycerol to hydroxyacetone was investigated. After the first test (Postcycle 1), the catalyst was recovered by decantation and it was washed with a 50/50 mixture methanol-water and dried at 100°C. The dried catalysts were calcined at 400 °C for 4 hours and finally reduced at 400 °C for 4 hours under hydrogen flow. The resultant reduced catalyst was used for the next cycle (Postcycle 2) under conditions that allowed to maintain the same glycerol/catalyst molar ratio used in the cycle 1. The same process of separation, washing and reactivation of the catalyst has been implemented for the Postcycle 3. As shown Fig. 10 the fresh 5%Cu/$ZrO_2$ gives at about 30% of glycerol conversion at 120 minutes of reaction. During the Postcycle 2 the

566 conversion of glycerol decreased to about 10% and in the third cycle the conversion
567 decreased to reach at about 5%.
568

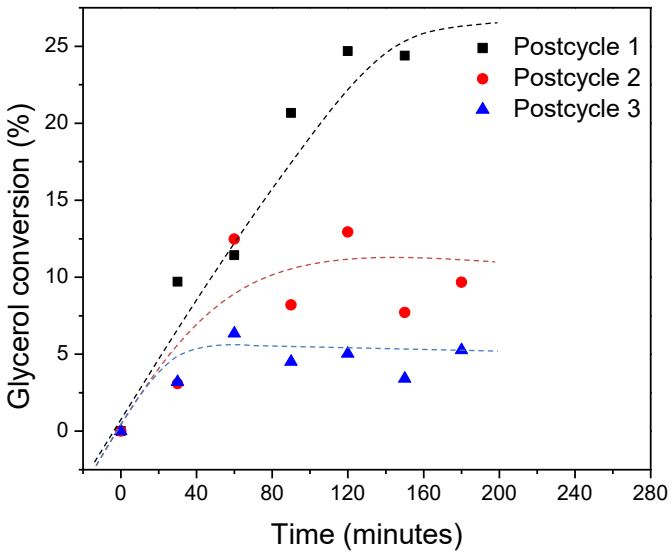


569

570 Fig. 10. 5%Cu/$ZrO_2$ catalyst recycling process in the glycerol dehydration. (Dashed lines
571 only serve to guide the eyes).
572

573 To identify the origin of the deactivation, the fresh and used 5% Cu/$ZrO_2$ catalysts
574 (reactivated by calcination-reduction) were characterized by nitrogen physisorption (Fig. S1
575 and Table 7) and $N_2O$ chemisorption (Fig. S2 and Table 7). In addition, X-ray diffraction
576 (Fig. S3) and scanning electron microscopy coupled to an energy dispersive X-ray
577 spectrometer (SEM-EDS) (Table 7) were performed. The EDS results indicate that copper
578 species are homogeneously distributed over $ZrO_2$ and there is no appreciable variation in the
579 atomic relationship Cu/Zr after each recycling (Table 7).
580
581
582

583 Table 7. Properties of the 5%Cu/$ZrO_2$ catalyst during the recycling process

| Sample | $S_{BET}$ ($m^2\ g^{-1}$) | $V_P$ ($cm^3\ g^{-1}$) | $d_p$ (nm) | $N_2O$ (μmol $N_2O\ g_{cat}^{-1}$) | Cu/Zr[a] |
|---|---|---|---|---|---|
| Fresh | 131 | 0.13 | 4.01 | 301 | 0.075 |
| Postcycle 1 | 128 | 0.15 | 4.24 | 286 | 0.090 |
| Postcycle 2 | 129 | 0.15 | 4.55 | 164 | 0.075 |
| Postcycle 3 | 116 | 0.14 | 4.86 | 170 | 0.079 |

584 [a] EDS

585

586 Change of the textural properties of 5%Cu/$ZrO_2$ material in the recycling was negligible
587 (Table 7). The total amount of chemisorbed $N_2O$ was progressively reduced between each
588 cycle (Fig. S2 and Table 7). Moreover, the X-ray diffraction of the used materials after each
589 reactivation indicates some sintering of copper species by the appearance of copper oxide
590 phase (Fig. S3). The observed sintering of copper particles after the catalytic cycles may
591 result in the loss of active site which can be considered as the main factor contributing to the
592 observed catalyst deactivation.

593

594 *3.4 DFT study*

595

596 To gain molecular insights and explain the support effects, adsorption energies of glycerol,
597 and hydroxyacetone were computed using DFT calculations. The effect of hydroxylation on
598 $Al_2O_3$ and $ZrO_2$ supports due to water dissociation, which is also related to Brönsted acid site
599 were also investigated. Three possible adsorption sites were considered on each surface i.e.
600 Cu site, Al or Zr site on support and interface site between Cu cluster and support. Here, we

report only adsorption at the most stable one. The adsorption energies were calculated using equation (9) and summarized in Table 8.

$$E_{ad} = E_{total} - E_{clean\ surface} - E_{adsorbate} \quad (9)$$

where $E_{ad}$ is adsorption energy, $E_{total}$ is energy of structures with glycerol/hydroxyacetone adsorption, $E_{clean\ surface}$ is energy of structures without glycerol/hydroxyacetone adsorption and $E_{adsorbate}$ is energy of isolated glycerol/hydroxyacetone molecule. The more negative values of $E_{ad}$, the stronger adsorption.

Table 8. Adsorption energies (kJ $mol^{-1}$) of glycerol and hydroxyacetone on Cu(111), $Cu_{13}/Al_2O_3(110)$, $Cu_{13}/ZrO_2(111)$, $Cu_{13}$/hydroxylated $Al_2O_3(110)$, and $Cu_{13}$/hydroxylated $ZrO_2(111)$ surfaces and Bader charge analysis of $Cu_{13}$ cluster. The corresponding adsorption structures are shown in Fig. 11.

| | **Adsorption energy (kJ $mol^{-1}$)** | | **Charge of $Cu_{13}$ cluster ($e^-$)** |
|---|---|---|---|
| | glycerol | hydroxyacetone | |
| **Cu(111)** | -100.12 | -102.13 | |
| **$Cu_{13}/Al_2O_3(110)$** | -337.77 | -252.71 | +0.13 |
| **$Cu_{13}$/hydroxylated $Al_2O_3(110)$** | -337.86 | -274.01 | +0.55 |
| **$Cu_{13}/ZrO_2(111)$** | -151.04 | -178.36 | -0.28 |
| **$Cu_{13}$/hydroxylated $ZrO_2(111)$** | -127.78 | -159.66 | -0.51 |

(a) Cu(111)

Orange atoms are Cu, red atoms are O, grey atoms are C and white atoms are H.

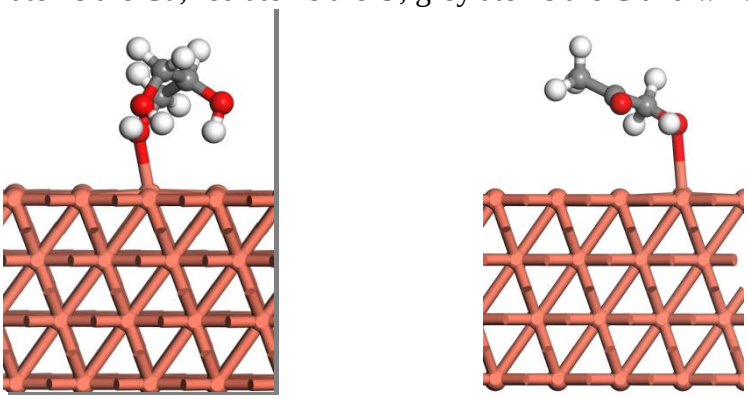

(b) $Cu_{13}/Al_2O_3(110)$

Purple atoms are Al.

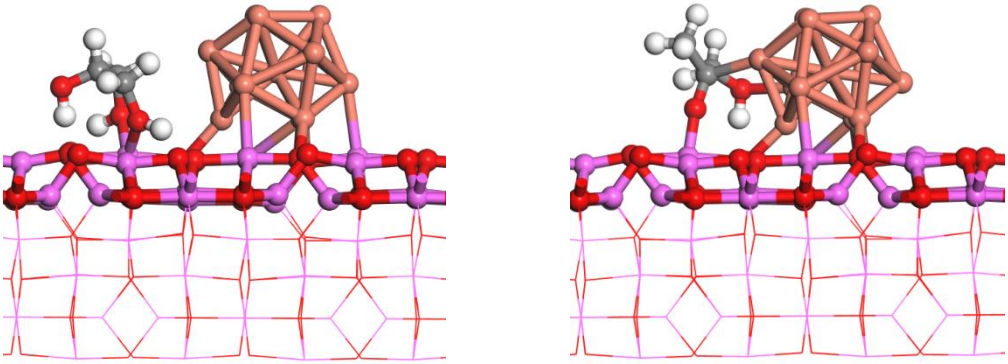

(c) $Cu_{13}$/hydroxylated $Al_2O_3(110)$

Blue atoms and light green atoms are O and H from hydroxylation, respectively.

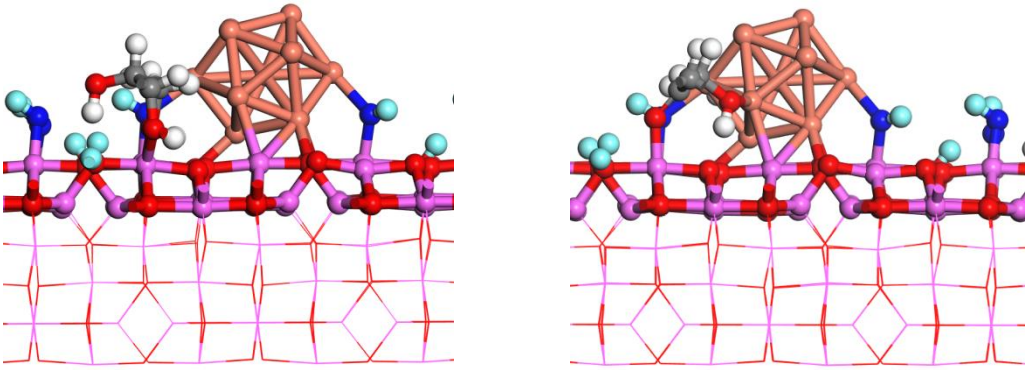

(d) $Cu_{13}/ZrO_2(111)$

Light green atoms are Zr.

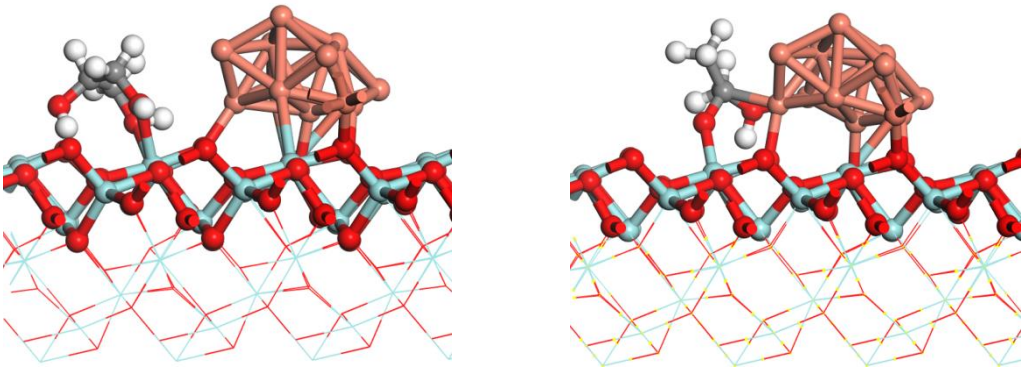

(e) $Cu_{13}$/ hydroxylated $ZrO_2(111)$
Blue atoms and dark green atoms are O and H from hydroxylation, respectively.

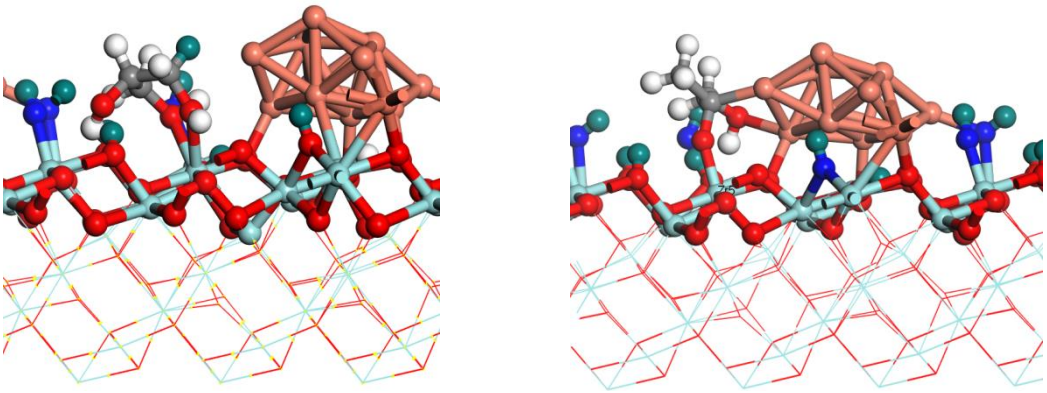

Fig. 11. Most stable adsorption structures of glycerol (left) and hydroxyacetone (right) on (a) Cu(111), (b) $Cu_{13}/Al_2O_3(110)$, (c) $Cu_{13}$/hydroxylated $Al_2O_3(110)$, (d) $Cu_{13}/ZrO_2(111)$, and (e) $Cu_{13}$/hydroxylated $ZrO_2(111)$ surfaces.

Glycerol and hydroxyacetone adsorption strength are in the order of Cu(111) < $Cu_{13}/ZrO_2(111)$ < $Cu_{13}/Al_2O_3(110)$. The relatively strong adsorption indicates that the support significantly facilitate interaction with glycerol and hydroxyacetone. The strong glycerol adsorption on $Cu_{13}/Al_2O_3(110)$ and $Cu_{13}/ZrO_2(111)$ surfaces could result from bidentate binding that both oxygen ends of glycerol molecule bond to the same metal atom

of support (Al or Zr) whereas monodentate binding occurs on Cu(111) surface (Fig. 11, left). Hydroxyacetone prefers to bind through oxygen atom of hydroxyl group on Cu(111) surface while it binds at the interface site where oxygen of carbonyl group interacts with metal site of support and oxygen of hydroxyl group interacts with copper site (Fig. 11, right). Thus, hydroxyacetone interaction on $Cu_{13}/Al_2O_3(110)$ and $Cu_{13}/ZrO_2(111)$ surfaces is significantly stronger than that on Cu(111) surface. As illustrated in Fig. 11, glycerol favours to adsorb at support's metal atom site locating adjacent to the Cu cluster and hydroxyacetone prefers to adsorb at the interface site requiring both support's metal atom site and Cu site. This suggests the vital synergistic role of the interface Cu-support as the active site and the significance of high copper particles dispersion, in which turn the increase of interfacial Cu-support sites. Hydroxylation on $Cu_{13}/Al_2O_3(110)$ and $Cu_{13}/ZrO_2(111)$ surfaces induce different impact on binding strength. Hydroxylation on $Cu_{13}/Al_2O_3(110)$ facilitates hydroxyacetone adsorption to be stronger while it weakens glycerol and hydroxyacetone adsorption on $Cu_{13}/ZrO_2(111)$, yet the favourable adsorption site and adsorption characteristic (monodentate/bidentate) are similar to those without hydroxylation.

Furthermore, Bader charge analysis (Table 8) of $Cu_{13}$ cluster was performed to better understand the effect of support. $Cu_{13}$ supported on $Al_2O_3$ lose electrons to $Al_2O_3$ showing positive charge while $Cu_{13}$ supported on $ZrO_2$ gain electrons from $ZrO_2$ showing negative charge. It is implied that $ZrO_2$ support shows stronger acidity compared to $Al_2O_3$ support. The hydroxylation increases the degree of electrons transfer from $Cu_{13}$ cluster to $Al_2O_3$ and from $ZrO_2$ to $Cu_{13}$ cluster resulting in higher positive charges of supported $Cu_{13}$ on $Al_2O_3$ and higher negative charge of supported $Cu_{13}$ on $ZrO_2$.

## 4. Discussion

To establish relationships between activity and structural parameters the copper based catalysts were evaluated in the glycerol dehydration. Fig. 12 illustrates a plot correlating the produced hydroxyacetone expressed in terms of μmol $m_{cat}^{-2}$ at 20% of conversion with the total number of exposed metallic copper species expressed in terms of the total quantity of chemisorbed $N_2O$ ($Y_{N2O}$, μmol $N_2O$ $m_{cat}^{-2}$) and with the total number of acid sites of the catalysts expressed in terms of μmol $NH_3$ $m_{cat}^{-2}$.

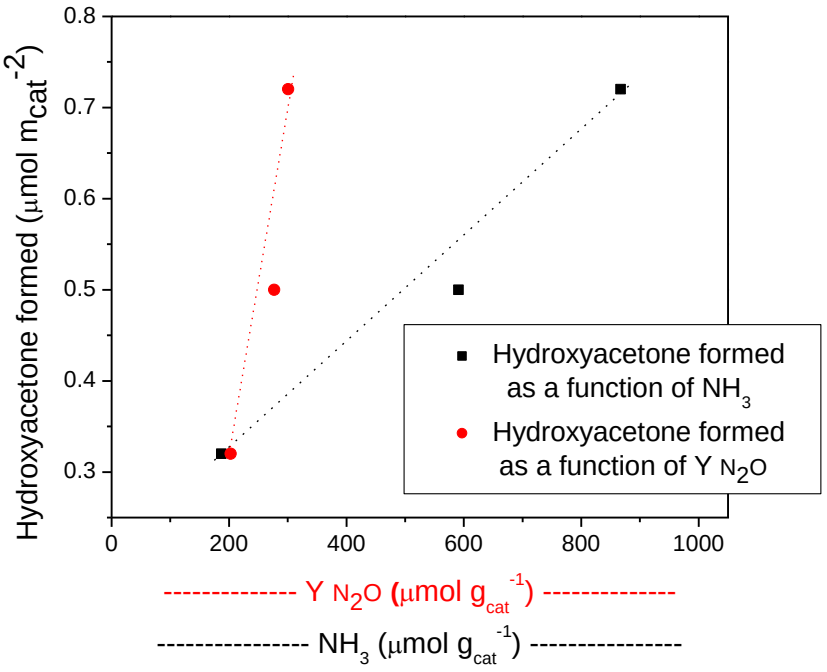


Fig. 12. Relationship between the total quantity of the produced hydroxyacetone versus exposed metallic copper atoms and the total quantity of acidic sites. (Dashed lines only serve to guide the eyes).

683 In the formation of hydroxyacetone stands out a lower sensitivity to the total number of acidic
684 sites compared to the total number of exposed copper atoms which is reflected in the quantity
685 of chemisorbed $N_2O$. A lower quantity of chemisorbed $N_2O$ exhibits a higher hydroxyacetone
686 yield when compared with the same quantity of acidic sites ($\mu$mol $NH_3$ $m_{cat}^{-2}$).
687
688 The calculation results also reveal that hydroxyacetone and glycerol bind stronger on
689 $Cu_{13}/Al_2O_3(110)$, $Cu_{13}/ZrO_2(111)$ surfaces compared to Cu(111) surface. Also, glycerol is
690 favourable to adsorb at support metal site close to copper cluster and hydroxyacetone is
691 favourable to adsorb at the interface copper-support site (Fig. 11 (right)). These results
692 suggest the synergistic role of acid sites (Al or Zr) of supports and copper cluster to promote
693 hydroxyacetone and glycerol interaction with surfaces. In addition, the active role of the
694 interfacial sites suggests the positive effects of highly dispersed Cu over support on catalytic
695 reactivity. The DFT calculations also indicate that stronger acidity of $ZrO_2$ may better
696 promote moderate interaction with intermediates while relatively weak acidity of $Al_2O_3$
697 results in too strong interaction with intermediates. Furthermore, the negative charges of
698 supported Cu cluster on $ZrO_2$ may indicate the number of acid sites increase with copper
699 introduction on $ZrO_2$ support.
700
701 It should be added that the highest kinetic constant indicates that the most active catalyst is
702 the 5%$Cu/ZrO_2$ catalyst. Particularly, $ZrO_2$ has been described as a preventive element for
703 sintering copper species and it is therefore considered to be a structural promoter [68]. It is
704 important to complement that the results of TPR indicate that the presence of $ZrO_2$ facilitates
705 the reduction of copper species, as well as the results of XRD, $N_2O$ chemisorption, EDS and

706 XPS which suggest that $ZrO_2$ support leads to a homogeneous distribution of copper species
707 and higher dispersion of the copper species compared with γ-$Al_2O_3$ and $SiO_2$. In addition,
708 pyridine infrared indicates that 5%Cu/$ZrO_2$ and 5%Cu/γ-$Al_2O_3$ catalysts present both acidic
709 sites of Lewis and Brönsted. For 5%Cu/$SiO_2$ only Lewis acid sites were found.
710
711 **5. Conclusions**
712
713 The dehydration reaction of glycerol to hydroxyacetone on copper based catalysts suggests
714 apparent first order kinetics. By $NH_3$-TPD, it has been observed that the 5%Cu/$ZrO_2$
715 exhibited the highest total quantity of acidic sites and total amount of $N_2O$ chemisorbed
716 suggesting higher dispersion of copper species compared with 5%Cu/γ-$Al_2O_3$ and
717 5%Cu/$SiO_2$ catalysts. XRD analysis suggests that copper species are finely dispersed on the
718 support. XPS analysis identified that copper species are found in metallic state at the catalyst
719 surface and the atomic ratio (Cu/M) (M= Si, Al or Zr) suggests that copper species are more
720 homogeneously distributed on $ZrO_2$ surface.
721
722 Complementary study of DFT indicates that both glycerol and hydroxyacetone adsorb
723 significantly stronger on $Cu_{13}$/γ-$Al_2O_3$ (110) and $Cu_{13}$/$ZrO_2$ (111) compared to Cu (111)
724 which further suggests that the active sites for glycerol and hydroxyacetone adsorption are
725 the metal support site and the dual site consisting of Al or Zr of the support ($ZrO_2$ and γ-
726 $Al_2O_3$) of the copper species.
727

The kinetic constants expressed in μmol $m_{cat}^{-2}$ indicate that the most active material for glycerol dehydration has been the 5%Cu/$ZrO_2$ catalyst. A linear correlation between the yield of hydroxyacetone expressed in terms of μmol $m_{cat}^{-2}$ with the total quantity of chemisorbed $N_2O$ and the total quantity of acidic sites suggest that the copper dispersion is a sensitivity factor for the activity in the glycerol dehydration.

The sintering of copper particles between each catalyst recycling step by the thermal activation process (calcination-reduction) is the main descriptor responsible for the lost in the activity for the 5%Cu/$ZrO_2$ in the recycling study in agreement with the progressive decrease in the total quantity of $N_2O$ chemisorbed after each cycle. In addition, the characterization by EDS did not indicate appreciable variation in the atomic Cu/Zr ratio between each one of the reactions in the recycling process.

**Acknowledgements**

The authors are grateful to FONDECYT 1201936 and FONDECYT 1180243 for the financial support. P.H would like to thank computational resources from NSTDA Supercomputer Center (ThaiSC) and National Nanotechnology Center (NANOTEC).

**References**

[1] S. Sato, M. Akiyama, R. Takahashi, T. Hara, K. Inui, M. Yokota, Appl. Catal A-Gen. 347 (2) (2008) 186-191.

[2] A. Corma, S. Iborra, A. Velty, Chem. Rev. 107 (6) (2007) 2411-2502.

[3] M. Dasari, P-P. Kiatsimkul, W. Sutterlin, G. Suppes, Appl. Catal. A-Gen., 281 (1-2) (2005) 225-231.

[4] J. Shabaker, G. Huber, J. Dumesic, J. Catal., 222 (1) (2004) 180-191.

[5] A. Corma, G. Huber, L. Sauvanaud, P. O´Connor, J. Catal. 247 (2), (2007) 307-327.

[6] S. Demirel, K. Lehnert, M. Lucas, P. Claus, Appl. Catal. B. 70 (1-4) (2007) 637-643.

[7] J. Barrault, Y. Pouilloux, J. Clacens, C. Vanhove, S. Bancquart, Catal. Today 75 (1-4) (2002) 177-181.

[8] A. Corma, S. Hamid, S. Iborra, A. Velty, J.Catal. 234 (2) (2005) 340-347.

[9] R. Mane, A. Yamaguchi, A. Malawadkar, M. Shirai, C. Rode, RSC Adv. 3 (37) (2013) 16499-16508.

[10] M. Aresta, A. Dibenedetto, F. Nocito, C. Ferragina, J Catal. 228 (1) (2009) 106-114.

[11] G. Yang, Y. Ke, H. Ren, C. Liu, R. Yang, W. Dong, Chem.Eng J. 283 (2016) 759-767.

[12] M. Mohamad, R. Awang, W. Zin, Am. J. Appl. Sci. 8 (11) (2001) 1135-1139.

[13] R. Disselkamp, B. Harris, T. Hart, Catal. Commun. 9 (13) (2008) 2250-2252.

[14] J. Ko, I. Kim, S. Yoo, B. Min, K. Kim, C. Park, J. Bacteriol. 187 (16) (2005) 5782-5789.

[15] S. Sato, D. Sakai, F. Sato, Y. Yamada, Chem. Lett. 41(9) (2012) 965–966.

[16] C. Chiu, A. Tekeei, W. Sutterlin, J.Ronco, G. Suppes, *AIChE J. 54 (9)* (2008) 2456-2463.

[17] A. Alhanash, E. Kozhevnikova, I. Kozhevnikov, Appl. Catal. A-Gen. 378 (1) (2010) 11-18.

[18] S. Zhu, X. Gao, Y. Zhu, Y. Zhu , H. Zheng, Y. Li, J. Catal. 303 (2013) 70-79.

[19] S. Zhu, X. Gao, Y. Zhu, W. Fan, J. Wang, Y. Li, Catal. Sci. Technol. 5 (2) (2005) 1169-1180.

[20] P. Hirunsit, C. Luadthong, K. Faungnawakij, RSC Adv. 15(5) (2015) 1118-11197.

[21] A. Bienholz, H. Hofmann, P. Claus, Appl. Catal. A-Gen. 391 (1-2) (2011) 153-157.

[22] S. Zhu, X.Gao, Y. Zhu, W. Fan, J. Wang, Y. Li, Catal. Sci. Technol. 5 (2) (2005) 1169-1180.

[23] H. S. Fogler, Elements of Chemical Reaction Engineering, 3rd edition, Prentice Hall International Series, 1988.

[24] O. Levenspiel, Chemical Reaction Engineering, 2nd edition, Wiley International edition, 1980.

[25] M. Digne, P. Sautet, P. Raybaud, P. Euzen, H. Toulhoat, J. Catal. 226 (2004) 54-68.

[26] P. Nortier, P. Fourre, A. B. M. Saad, O. Saur, J.C. Lavalley, Applied Catalysis 61 (1990) 141-160.

[27] X. Krokidis, P. Raybaud, A. E. Gobichon, B. Rebours, P. Euzen, H. Toulhoat, The Journal of Physical Chemistry B 105(22) (2001) 5121-5130.

[28] J. P. Chou, H. Y. T. Chen, C. R. Hsing, C. M. Chang, C. Cheng, and C. M. Wei, Phys. Rev. B 80 (2009) 165412.

[29] M. J. Piotrowski, P. Piquini, J. L. F. da Silva, Phys. Rev. B 81 (2010) 155446.

[30] T. T. Li, C. He, W.X. Zhang, M. Cheng, Applied Surface Science 479 (2019) 39-46.

[31] W. Zeng, J. Tang, P. Wang, Y. Pei, RSC Advances 6(61) (2016) 55867-55877.

[32] S. Chen, X. Chen, H. Zhang, Journal of Materials Science **52**(6) (2017) 3162-3168.

[33] H. Gao, RSC Advances, 2016. 6(105): p. 102914-102923.

[34] P. Hirunsit, K.-ichi Shimizu, R. Fukuda, S. Namuangruk, Y. Morikawa, M. Ehara, The Journal of Physical Chemistry C 118(15) (2014) 7996-8006.

[35] C. H. Hu, C. Chizallet, C. M. Maury, M. C. Valero, P. Sautet, H. Toulhoat, P. Raybaud, Journal of Catalysis 274 (1) (2010) 99-110.

[36] C. Dessal, A. Sangnier, C. Chizallet, C. Dujardin, F. Morfin, J. L. Rousset, M. Aouine, M. Bugnet, P. Afanasiev, L. Piccolo, Nanoscale 11 (2019) 6897-6904.

[37] P. Lackner, J. Hulva, E. M. Köck, W. M. Schmölzer, J. J. Choi, S. Penner, U. Diebold, F. Mittedonfer, J. Redinger, B. Klötzer, G. S. Parkinson, M. Schmid, J. Mater. Chem. A 6 (2018) 17587-17601.

[38] G. Kresse, J. Furthmüller, Computational Materials Science **6**(1) (1996) 15-50.

[39] G. Kresse, J. Furthmüller, Physical Review B, **54**(16) (1996) 11169-11186.

[40] J.P. Perdew, K. Burke, M. Ernzerhof, Physical Review Letters **77**(18) (1996) 3865-3868.

[41] P.E. Blöchl, Physical Review B 50(24) (1994) 17953-17979.

[42] G. Kresse, D. Joubert, Physical Review B 59(3) (1999) 1758-1775.

[43] S. Grimme, J. Comput. Chem. 2006, 27, 1787-1799.

[44] S. Grimme, J. Antony, S. Ehrlich, H. Krieg, J. Chem. Phys. 2010, 132, 154104.

[45] C.L. Fu, K.M. Ho, Physical Review B 28(10) (1983) 5480-5486.

[46] H.J. Monkhorst, J.D. Pack, Phys. Rev. B, 13(12) (1976) 5188-5192.

[47] G. Henkelman, A. Arnaldsson, H. Jonsson, Comput. Mater. Sci. 36 (2006) 354−360.

[48] E. Sanville, S. D. Kenny, R. Smith, G. Henkelman, J. Comput. Chem. 2007, 28, 899−908.

[49] W. Tang, E. Sanville, G. Henkelman, J. Phys.: Condens. Matter 2009, 21, 084204

[50] K. Sing, Pure Appl.Chem.,54 (11), 2201-22l8.

[51] F. López, A. Bueno, M. Illán, Appl. Catal. B-Environ. 84(3-4) (2008) 651-658.

817 [52] R. Friedman, J. Freeman, F. Lytle, J. Catal. 55 (1) (1978) 10-28.

818 [53] J. Aguado, J.M. Escola, M.C. Castro, B. Paredes, Appl Catal A Gen 284 (2005) 47–57.

819 [54] B. Chakraborty, B. Viswanathan, Catal Today 49 (1999) 253–260.

820 [55] S. E. Voltz, A. E. Hirscheler, A. Smith, J. Phys. Chem. 64 (1960) 1594.

821 [56] S. Triwahyono, T, Yamada, H. Hattori, Appl. Catal., A 2003, 242, 101-109.

822 [57] A. Gervasini, S. Bennici, Appl. Catal. A-Gen.281 (1-2) (2005) 199-205.

823 [58] Z. Liu, M. Amiridis, Y. Chen, J. Phys. Chem. B. 109 (3) (2005) 1251-1255.

824 [59] A. Y. Yin, J. W. Qu, X. Y. Guo, W. L. Dai, K. N. Fan, Appl. Catal. A, 400 (2011) 39–
825 47.

826 [60] I.C. Freitas, S. Damyanova, D.C. Oliveira, C.M.P. Marques, J.M.C Bueno, Journal of
827 Molecular Catalysis A: Chemical 381 (2014) 26-37.

828 [61] Y. Chen, L. Dong, Y. Jin, X. Bing, J. Weijie, Stud. Surf. Sci. Catal., 101, (1996) 1293-
829 1302.

830 [62] F. Severino, J. Brito, O. Carias, J. Laine, J. Catal., 102 (1) (1986) 172-179.

831 [63] G. Aguila, F. Gracia, J. Cortés, P. Araya, Appl. Catal. B-Environ. 77(3-4) (2008) 325-
832 338.

833 [64] M. Manzoli, R. Di Monte, F. Boccuzzi, S. Coluccia, J. Kaspar, Appl. Catal. B. 61 (3-4)
834 (2005) 192-205.

835 [65] S. Velu, K. Suzuki, C. Gopinath, H. Yoshida, T. Hattori, Phys. Chem. Chem. Phys. 4
836 (10) (2002) 1990-1999.

837 [66] W. Suprun, M. Lutecki, T. Haber, H. Papp, Journal Molecular Catalysis A: Chemical
838 309 (2009) 71-78.

839 [67] J. Ten Dam, U. Hanefeld, ChemSusChem 4 (10) (2011) 1017-1034.

[68] J. Agrell, H. Birgersson, M. Boutonnet, I. M. Cabrera, R. Navarro, J.L.G. Fierro, J. Catal. 219 (2) (2003) 389-403.